ASTROBIOLOGY
Volume 8, Number 5, 2008

DOI: 10.1089/ast.2007.0217

Special Paper

The 2005 MARTE Robotic Drilling Experiment in Río Tinto, Spain: Objectives, Approach, and Results of a Simulated Mission to Search for Life in the Martian Subsurface

Carol R. Stoker,[1] Howard N. Cannon,[1] Stephen E. Dunagan,[1] Lawrence G. Lemke,[1] Brian J. Glass,[1] David Miller,[2] Javier Gomez-Elvira,[3] Kiel Davis,[4] Jhony Zavaleta,[1] Alois Winterholler,[2] Matt Roman,[2] Jose Antonio Rodriguez-Manfredi,[3] Rosalba Bonaccorsi,[1] Mary Sue Bell,[5] Adrian Brown,[6] Melissa Battler,[7,*] Bin Chen,[6] George Cooper,[8] Mark Davidson,[9] David Fernández-Remolar,[3] Eduardo Gonzales-Pastor,[3] Jennifer L. Heldmann,[1] Jesus Martínez-Frías,[3] Victor Parro,[3] Olga Prieto-Ballesteros,[3] Brad Sutter,[5] Andrew C. Schuerger,[10] John Schutt,[11] and Fernando Rull[3]

Abstract

The Mars Astrobiology Research and Technology Experiment (MARTE) simulated a robotic drilling mission to search for subsurface life on Mars. The drill site was on Peña de Hierro near the headwaters of the Río Tinto river (southwest Spain), on a deposit that includes massive sulfides and their gossanized remains that resemble some iron and sulfur minerals found on Mars. The mission used a fluidless, 10-axis, autonomous coring drill mounted on a simulated lander. Cores were faced; then instruments collected color wide-angle context images, color microscopic images, visible–near infrared point spectra, and (lower resolution) visible–near infrared hyperspectral images. Cores were then stored for further processing or ejected. A borehole inspection system collected panoramic imaging and Raman spectra of borehole walls. Life detection was performed on full cores with an adenosine triphosphate luciferin-luciferase bioluminescence assay and on crushed core sections with SOLID2, an antibody array-based instrument. Two remotely located science teams analyzed the remote sensing data and chose subsample locations. In 30 days of operation, the drill penetrated to 6 m and collected 21 cores. Biosignatures were detected in 12 of 15 samples analyzed by SOLID2. Science teams correctly interpreted the nature of the deposits drilled as compared to the ground truth. This experiment shows that drilling to search for subsurface life on Mars is technically feasible and scientifically rewarding. Key Words: Mars—Drilling—Mission simulation—Field test—Life detection—Subsurface biology. Astrobiology 8, 921–945.

[1]NASA Ames Research Center, Moffett Field, California.
[2]School of Aerospace & Mechanical Engineering, University of Oklahoma, Norman, Oklahoma.
[3]Centro de Astrobiología, CSIC/INTA, Madrid, Spain.
[4]Honeybee Robotics Spacecraft Mechanisms Corporation, New York, New York.
[5]NASA Johnson Space Center, Houston, Texas.
[6]SETI Institute, Mountain View, California.
[7]University of New Brunswick, Canada.
[8]Civil & Environmental Engineering, University of California Berkeley, Berkeley, California.
[9]Department of Geosciences, Princeton University, Princeton, New Jersey.
[10]Department of Plant Pathology, University of Florida, Gainesville, Florida.
[11]Mars Institute, Moffett Field, California.
[*]Present address: University of Western Ontario, Centre for Planetary Science & Exploration, London, Ontario, Canada.

1. Introduction

Most familiar life-forms on Earth live on the surface where liquid water, sunlight, and the essential chemical elements and nutrients for life are abundant. However, such environments are not found anywhere else in the Solar System. The foremost requirements for life are liquid water and a source of energy. On other Solar System bodies, liquid water is absent at the surface, but evidence suggests subsurface water may exist on Mars (Clifford and Parker, 2001; Heldmann and Mellon, 2004; Malin *et al*., 2006), Europa (Pappalardo *et al*., 1999), and Enceladus (Hansen *et al*., 2006). In addition to liquid water, subsurface life on other worlds would need a source of chemical energy as a basis for primary production. Examples of subsurface life relying solely on chemical energy on Earth are rare (*e.g*., Stevens, 1997, 2002), but some ecosystems have been described that appear to exist on chemical energy independently of the surface (Stevens and McKinley, 1995, 2000; Pedersen, 2001; Takai *et al*., 2001; Chapelle *et al*., 2002).

The surface of Mars is hostile to both microbial metabolism and the preservation of organic compounds. Typical surface temperature and pressure prevent liquid water formation, ultraviolet light from the Sun is intense, and reactive oxidants may be present that destroy organics (Klein, 1979; Zent and McKay, 1994). However, many authors have suggested that the subsurface of Mars might be conducive to life (*e.g*., Boston *et al*., 1992, 2001; Carr, 1996; Nealson, 1997; Shock, 1997; Sleep and Zahnle, 1998; Fisk and Giovannoni, 1999).

The drilling depth required to search for life on Mars is an important factor to consider. Theoretical considerations (Clifford and Parker, 2001; Clifford, 2003) point to liquid water at a few to several kilometers deep. Gully features that are found at mid and high latitudes (Malin and Edgett, 2000; Malin *et al*., 2006) may be signatures of shallower aquifers, though the implied depths [200 m to 1 km (Heldmann and Mellon, 2004)] are still beyond foreseeable robotic drilling capabilities. Furthermore, there are alternative explanations for the martian gullies (Christensen, 2003) that don't involve an aquifer, and the existence of any subsurface aquifer on Mars is only theoretical.

Shallow drilling may be used to access an important region for searching for modern life. The icy deposits in the northern plains of Mars (Boynton *et al*., 2002) could plausibly have experienced liquid water at or near the surface in geologically recent times, which motivated scientists to choose this region for the Phoenix Mars lander. Periodic changes in Mars orbit (obliquity and phasing of perihelion) cause large variations in the amount of solar insolation in Mars' polar regions (Murray *et al*., 1973). Consequently, over the last 5 million years, the northern plains of Mars have experienced many epochs where thermodynamic conditions allowed liquid water to form (Haberle *et al*., 2001; Richardson and Michna, 2005). Furthermore, clement conditions repeat over fairly short timescales. Today, perihelion (Ls = 257) almost coincides with southern summer solstice (Ls = 270), and therefore the specific intensity of summer sunlight is higher in the south polar region than in the north. The solar longitude that coincides with perihelion precesses through a complete 360° cycle in 50,000 years. When perihelion occurs during northern summer, the available summer insolation is 30% higher than at present, and conditions may allow melting of high-latitude ground ice (Richardson and Michna, 2005).

Over the past 5 million years, the available insolation has changed even more dramatically as the obliquity varied between 15° and 35° (Laskar *et al*., 2004). During high obliquity, the specific intensity of the maximum summer Sun in the north polar regions was 2.5 times the present value, with polar summertime temperatures correspondingly higher. Drilling several meters' depth into the icy northern plains deposits could provide samples that contain a record of these warmer periods. Drilling is important because near-surface samples (as accessed by the Phoenix mission), which currently are ice rich, were ice free during warmer epochs (Mellon and Phillips, 2001) and so subject to the oxidizing conditions that destroy any record of biology.

Drilling may be equally important for finding evidence of life on Mars from the early martian epoch when liquid water was stable at the surface [see Carr (1996) for a review]. The oxidizing conditions on the martian surface may destroy organics in the soil to depths of up to several meters (Bullock *et al*., 1994). The surfaces of rocks are weathered by exposure to these oxidants, and grinding them to remove the weathered coating has been important for understanding the unaltered rock composition (Arvidson *et al*., 2004). Drilling may provide access to pristine samples that contain an organic record of life.

1.1. The MARTE project: exploring for subsurface life at a Mars analog site

The Mars Astrobiology Research and Technology Experiment (MARTE) conducted a search for a subsurface biosphere near the Río Tinto headwaters as an analogue for searching for life on Mars. Funded by the NASA Astrobiology Science and Technology for Exploring Planets (ASTEP) program, MARTE had two mutually supportive goals: (1) search for subsurface life at a site not previously characterized and (2) develop and test robotics technology for searching for life on Mars. The search for subsurface life in a terrestrial field site with the use of conventional drilling technology and extensive laboratory analysis of samples served as an important learning experience that will help to guide the design of a robotic system to drill and search for life. The analysis and interpretations from the conventional drilling also provided important ground truth to compare results from the robotic drilling. Hereafter, we refer to the conventional deep-drilling experiment as ground truth drilling.

The Río Tinto is a river sourced in the Iberian pyrite belt in southwestern Spain, one of Earth's largest volcanogenic massive sulfide provinces (Leistel *et al*., 1998). Massive bodies of iron and copper sulfides, as well as minor quantities of lead and zinc, constitute the main mineral ores. The Iberian pyrite belt corresponds to an area of Devonian-Carboniferous volcanic and sedimentary rock that contains about 90 massive polymetallic sulfide deposits. This area, about 250 km long and 60 km wide, trends westward from near Seville (Spain) to southern Portugal. The Río Tinto deposit comprises 10 massive sulfide bodies in the center of the mining area (Carvalho *et al*., 1999). The stratigraphy of the Iberian pyrite belt has 3 major units. From bottom to top they

are the Phyllite-Quartzite Group, the Volcano-Sedimentary Complex, and the Flysch Group (Carvalho *et al*., 1999; Sáez *et al*., 1999).

Figure 1 shows the geographic location of the river and the drill sites. The river flows 100 km from Peña de Hierro (Iron Mountain), in the core of the Iberian pyrite belt, to the Atlantic Ocean, and its basin covers an area of around 1700 km^2. The river flows through an important mining district that has been exploited for over 5000 years and is among the "King Solomon's Mines" of the ancient world. Paleolithic inhabitants of the area followed by Phoenicians and Romans mined intensively in the area for 3000 years, and today mining for gold, zinc, and copper continues.

The waters of the Río Tinto are the color of dark red wine, a result of the high concentration of ferric iron maintained in solution by an acidic pH (mean 2.3). The source of the acidic conditions in the river is the sulfuric acid released in the oxidation of pyrite, while the iron in solution in the river serves as a buffer on the pH (Fernández-Remolar *et al*., 2003; Gómez *et al*., 2004). Although the acidic waters of the Río Tinto were once thought to result from environmental damage due to mining, further research (Fernández-Remolar *et al*., 2004) showed that a similar environment has existed for at least 10^5 years and, thus, predates human activity. The extreme acidity and the high concentration of heavy metals are the direct consequence of biological processes of iron- and sulfur-oxidizing microbes (bacteria and archaea) that grow in the metallic sulfide deposits of the Iberian pyrite belt (Lopez-Archilla *et al*., 2001; González-Toril *et al*., 2003).

The river headwaters begin just south of Peña de Hierro, a volcanogenic massive sulfide site where acidic waters, already carrying high ionic loads and at low pH, emerge from underground as seeps. This contrasts with typical acid mine drainage systems, where acid is generated in the interaction of oxygenated meteoric water with mine tailings at the surface (Maier, 2000).

The Río Tinto area is an important Mars analogue to the terrain visited by the Mars Exploration Rover Opportunity (Fernández-Remolar *et al*., 2005; Amils *et al*., 2007). Río Tinto's acidic and aqueous conditions produce similar mineralogies to those observed on Mars (Klingelhöfer *et al*., 2004). In fact, the similarity of many terrestrial mine deposits to the minerals found on Mars is notable (Burt *et al*., 2006). During the hot summers experienced in the area, evaporation of Río Tinto waters results in crusts of jarosite and related sulfate minerals. Ironstone and crystalline hematite are found in both modern and ancient river deposits.

Artesian springs that source the Río Tinto emerge on the southern flank of Peña de Hierro on steep slopes. At their source, many of these seeps are at very low pH (0–1), which indicates possibly acidic groundwater. These springs may have analogues in the gullies on Mars that appear to be seeps outcropping on steep slopes (Malin and Edgett, 2000; Heldmann and Mellon, 2004). Sampling a martian groundwater system that sources these springs would be a desirable target for a future Mars deep drilling mission, so the MARTE ground truth drilling has provided a useful analog experience.

To explore the hypothesis of a subsurface microbial ecosystem at Río Tinto that derives chemical energy from the metabolism of iron and reduced sulfur minerals, we selected drill sites where groundwater intersects these minerals. Figure 2 is a local geologic map of the drill area. Workers in the field identified sulfide deposits, and transverse electromagnetic sounding was conducted to map groundwater flow paths (Jernsletten, 2005). A mine pit crater on Peña de Hierro (Fig. 2 and Fig.1c) has exposed a sulfide ore deposit beginning at ~60 m below ground level. The pit is filled with water to 90 m below the surface, which reveals the level of the water table. A network of artesian springs outcrop south of (downhill from) this pit crater. Some spring-fed streams (mapped purple in Fig. 2) have low pH where they outcrop, but other surrounding springs have normal pH at outcrop, which suggests that the groundwater that produces low pH springs interacts with the subsurface sulfide ore body. For the ground truth drilling experiment, drill sites were chosen in a location near the northeast edge of the mine pit crater to sample the sulfide where 2 faults intersect and provide groundwater flow paths.

The MARTE ground truth drilling performed core drilling with aseptic sample collection and analysis during 2003–2004. With the use of commercial coring, a series of boreholes were drilled and springs were sampled to characterize subsurface life and its energy sources and by-products (Stoker *et al*., 2004, 2005). Boreholes 1 (60 m in organic rich shale), 4 , and 8 (160 m each in sulfide ore deposit) were drilled. Drilling depths were sufficient to encounter groundwater in each case. With the use of extensive conventional laboratory work, aseptic samples obtained from the cores were analyzed for the presence of microbes, the environmental resources available to them, and the by-products of their metabolism. Results of this analysis are summarized in Fernández-Remolar *et al*. (2008) and reveal evidence of an anaerobic chemolithoautotrophic biosphere, a unique system that derives energy from the metabolism of metallic sulfides.

In September of 2005, a simulation of a Mars drilling mission, which used a fully robotic approach, was performed at Borehole 7 (Fig. 2). The goals of this experiment were (1) to search for evidence of subsurface life as well as associated morphological and mineralogical evidence of aqueous alteration that may be associated with life signatures, (2) to demonstrate the robotic technologies for drilling, sample handling, and remote inspection of samples to identify locations for life-detection assays, and (3) to demonstrate remote life detection by a science team following a blind protocol.

Site selection for the robotic drilling experiment was driven by the desire to find a location where relevant analogues to Mars mineralogies occurred within 10 m of the surface, the maximum depth of the MARTE drill. A desirable site would also be near the location of the ground truth drilling experiment to allow comparison with those results. The site chosen, called Borehole 7 (see Fig. 2), was near Boreholes 4 and 8, both of which allowed access to the sulfide-water interaction zone for sampling in the ground truth drilling campaign. Although Borehole 7 was much shallower than 4 and 8, it drilled gossanized material near the surface where water and chemical oxidation has converted the sulfide into alteration products, including sulfate, hematite, and goethite. Familiar to exploration geologists, gossan at the surface is typically an indicator of subsurface sulfides, since surface weathering converts sulfides to their alteration products. Possible fossil biosignatures were found in these strata during the ground truth drilling experiment (Fernández-Remolar *et al*., 2008).

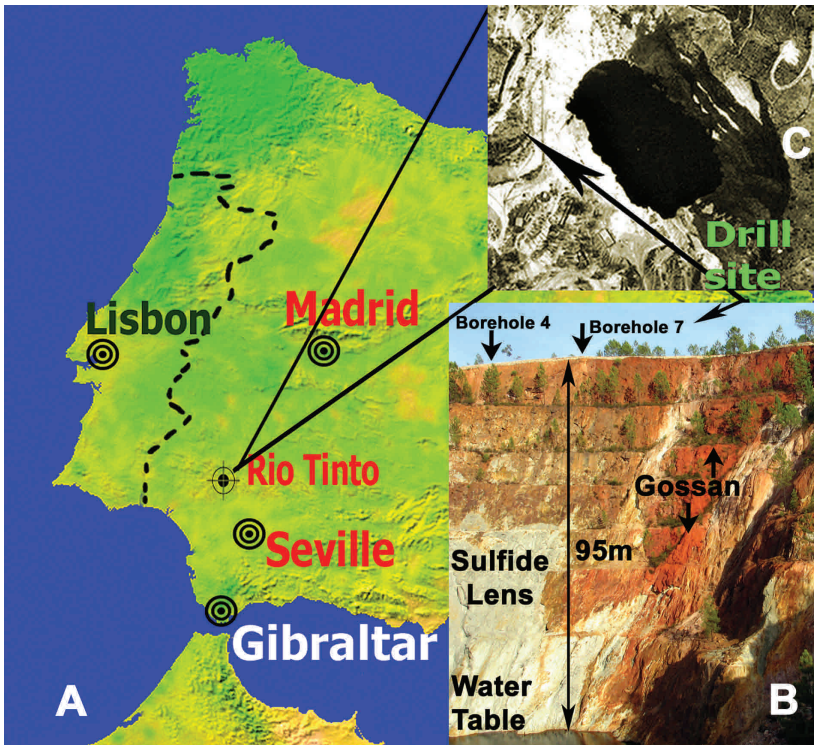

FIG. 1. (**A**) Map that shows the geographic location of the Río Tinto in southwest Spain. The field site is on Peña de Hierro north of the river's headwaters. (**B**) Aerial photograph showing the field site location (black arrow). (**C**) The drill site (Borehole 7) was located near the edge of a mine pit crater shown in cross section. The drill perforated the red gossanized layer at the surface. Beneath and to the left of this site the grey deposit is massive sulfide sampled in Boreholes 4 and 8. The light-toned unit to the right of the drill site is rich in sulfates and clays. Water fills the base of the crater at 95 m below the surface.

Below, we provide an overview of the 2005 MARTE robotic drilling mission simulation. We first focus on a description of the robotic drilling and sample handling systems as well as the instrument payload. Next, we summarize the experiment results, including drill and other robotic system performance and science team interpretations as compared with ground truth. Finally, we present lessons learned and guidance for future Mars drilling missions derived from the experiment results.

2. Mission Description

Development of drilling, sample handling, and life-detection technologies was a key goal of the MARTE project. The MARTE drilling platform (Fig. 3) is one of the most sophisticated robotic systems ever assembled for drilling and core sample analysis, and it is also the most complete system ever developed for planetary drilling. The discussion below provides details of all the subsystems incorporated onto the platform.

2.1. Drill Core Service Module (DCSM)

In a flight mission, the Mars lander provides interfaces for power, data, and mechanical mounting for the drill; a core sample handling system; science instruments; and related components. The DCSM support module, built at NASA Ames Research Center, provides these same interfaces for the MARTE hardware. To fit within the allowable time and cost constraints, however, no attempt was made to make the DCSM "flight-like" in terms of mass, volume, reliability, or style of construction; rather, it was designed to accommodate the other subsystems.

Figure 4 shows the DCSM design. It has three main components: a base structure, (the main body of the module), mounting Deck-A, and mounting Deck-B. The base structure is a hexagonal-shaped platform (1.5 m per side) with a truss system designed to distribute the load uniformly at three points on the ground by way of three peripheral, triangulated, and adjustable-length legs. Deck-A is mounted on the base structure and connected to it by a rotating pin that allows 360° of rotation via rollers that follow a circular path on top of the base structure's reinforced aluminum plate. This allows the drill and other instruments on the Borehole Inspection System to access the same hole. Deck-A′ houses most of the remote science instruments and the Core Sample Handling System (CSHS). Deck-A′ is made from an aluminum composite honeycomb plate mounted on top of Deck-A with special mounts to isolate vibrations introduced into the DCSM structure by drilling. Deck-A houses other important components such as the Borehole Inspection System (BHIS), the drill, and other supporting equipment such as power supplies and instrument electronics. Deck-B does not rotate. A cage mounted over the structure provides additional rigidity and stabilization of the drill mast.

2.2. MARTE drill

The MARTE drilling system, described extensively in Cannon *et al*. (2007), was built by Honeybee Robotics. The 10 m MARTE drill is a highly automated drill and core retrieval system largely based on a similar robotic drilling system built and tested by Honeybee Robotics for the Mars Technology Program (MTP) from 2001–2003. The original system was designed to address martian subsurface access requirements by acquiring stratigraphically maintained core samples in both solid and unconsolidated material down to

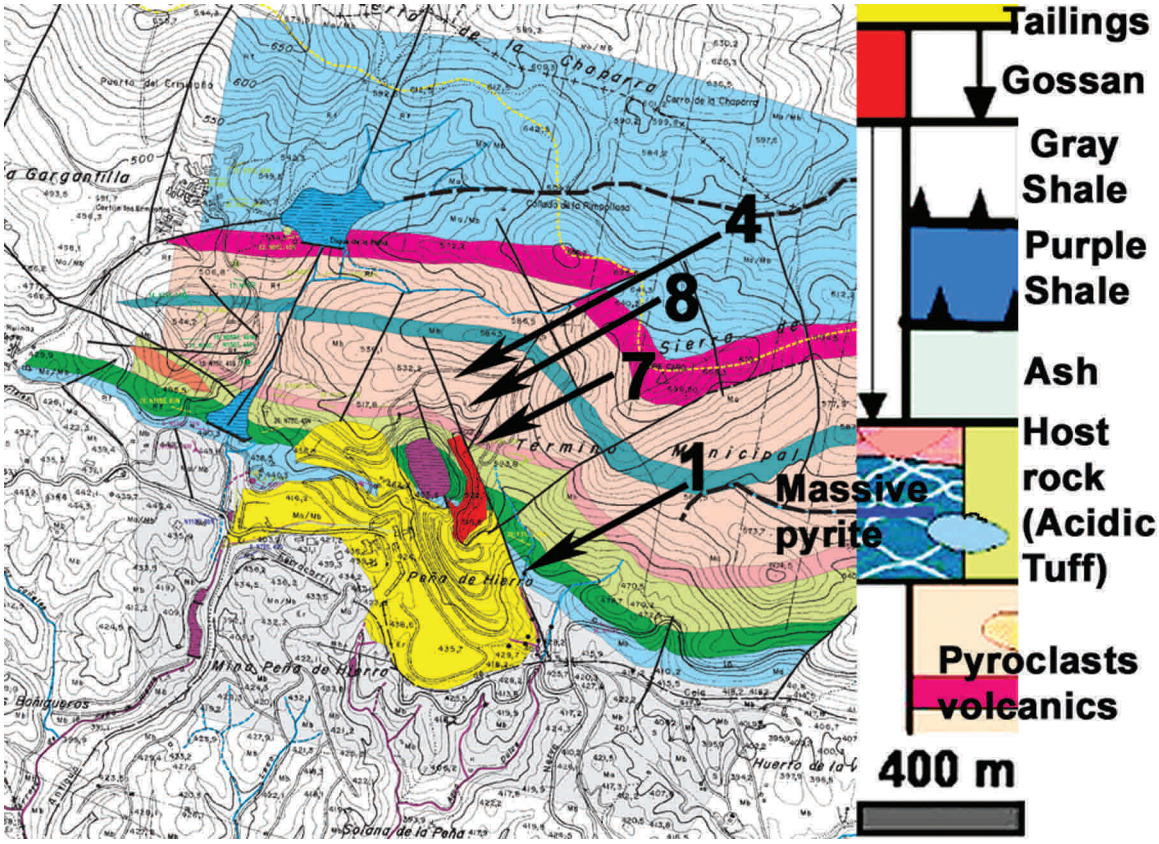

FIG. 2. Local geologic map produced from field observations shows the locations of the robotic drilling site (7) and the boreholes (1, 4, and 8) drilled as part of the MARTE ground truth drilling campaign.

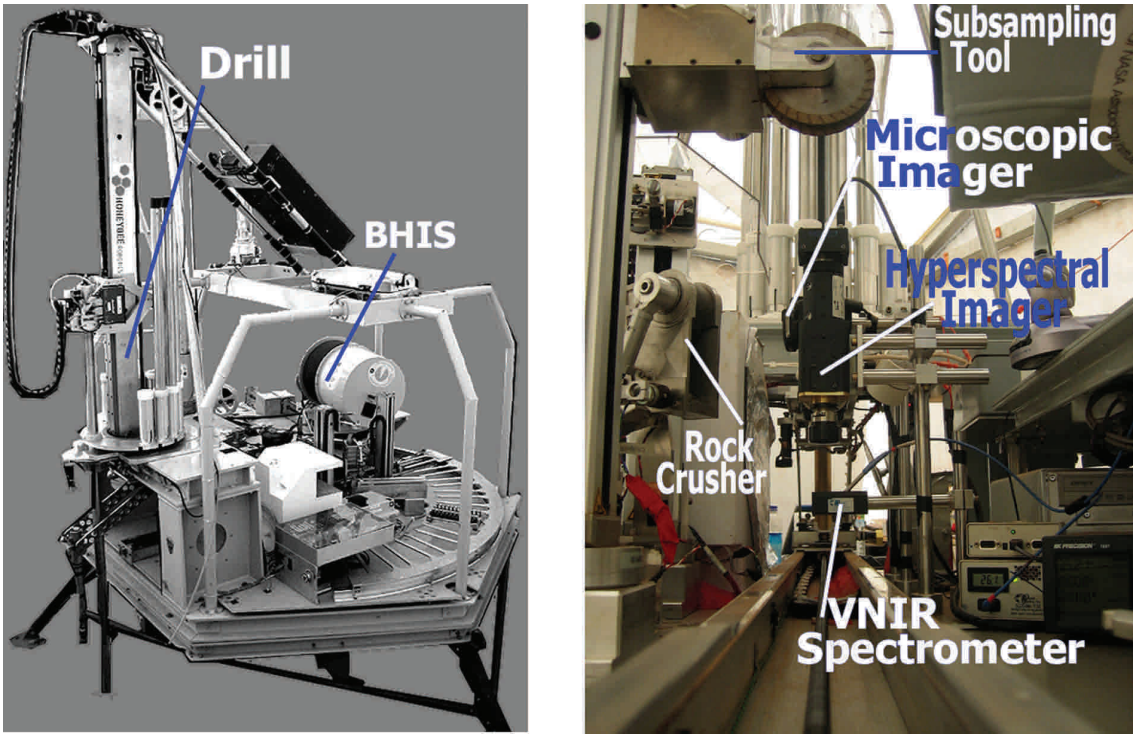

FIG. 3. Two views of the MARTE drill platform. **Left:** A wide-angle view showing the complete lander platform. **Right:** A view along the lander deck showing the linear rail for the core clamp, the remote sensing instruments, and the sampling saw and rock crusher.

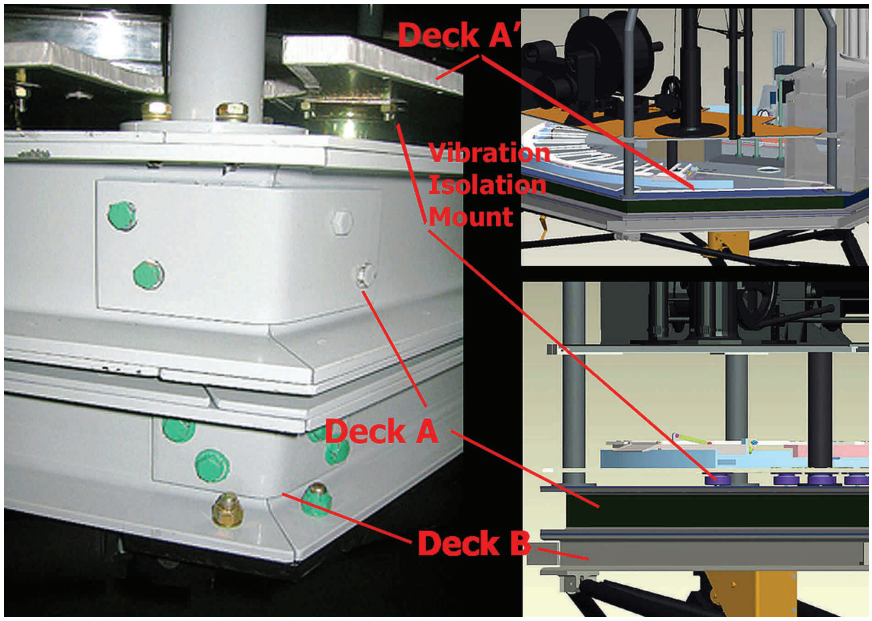

FIG. 4. **Left:** Photograph of the corner of the lander showing the 3 decks: Deck-B, which serves as the fixed-base structural plate; Deck-A, which rotates on Deck-B, allowing the drill and the BHIS to access the hole; and Deck-A′, which is vibration-isolated from Deck-A and serves as the mounting platform for science instruments that allows them to operate during drilling operations. **Right top:** CAD model view of the DCSM design. Elevated above Deck-A′ is a partial deck holding the BHIS. **Right bottom:** Detail of the 4-deck structure.

10 m depths. The MTP-sponsored drilling effort culminated with two field tests of a prototype system at the Golden Sunset Mining and Milling Co. (outside Phoenix, Arizona) in December 2002 and February 2003. During the second field test, a borehole depth of 8.3 m was achieved with Mars "flight-like" power and thrust levels (<100 W and <450 N).

Table 1 shows the drill specifications, and Fig. 5 shows the drill. The 10-axis system is designed for subsurface core sample recovery and hand-off from depths of up to 10 m. The MARTE drill produces rock cores 27 mm in diameter and 250 mm long while creating a 48 mm diameter borehole. The nominal core and borehole diameter dimensions were chosen to be compatible with a commercial coring system (Boart Longyear AQTK), which thus allows for use of a commercial drill to obtain cores for testing other subsystems. The drilling mechanism utilizes dry rotary cutting techniques, including both carbide drag cutters and mono-crystal diamonds. An auger-type chip removal system moves the cuttings away from the drill bit and into a chip reservoir located inside the lead drill tube, which is emptied upon removal from the borehole. A core hand-off subsystem removes the acquired core from the lead drill tube and delivers it to a core clamp for sample preparation and delivery to scientific instruments for analysis. The system is designed to operate with an average power of 150 W during nominal drilling operations. Highly integrated sensor feedback controls on all drilling axes allow for autonomous operation. The drilling mechanism has 7 degrees of freedom as follows: the auger axis rotates the drill bit, the z axis provides weight on bit and bit penetration, the drill head and string actuators lock and unlock the drill segments, the index axis places the drill segment feeder under the drill head for adding or subtracting segments from the borehole, the core break-off axis captures and retains cores, and the clamp holds drill segments in place during segment addition and subtraction.

A drilling depth of 10 m is accomplished via a 1.5 m lead drill string, which is followed by 10 identical 1 m drill segments. Segments are added into the borehole when the drill head reaches the lower limit of the z axis. Upon retrieval, each drill segment is autonomously stored in the index cache as it comes to the surface.

Extensive laboratory tests of Río Tinto rocks obtained during ground truth drilling were used to determine the best bit configuration for the drill. Two end-member rock types were tested: gossan and volcanosedimentary rocks. Depending on the properties of the rock drilled, carbide drag cutters or

TABLE 1. DRILL CHARACTERISTICS

System component	*Characteristics*
Drill volume occupied	2.1 m × 0.58 m × 0.77m
Drill mass	55 kg
Power	200 W maximum, 150 W average
Components	1.5 m lead drill string, 10 one-meter drill-string segments
Thrust	2670 N maximum
Auger speed and torque	150 rpm maximum auger speed, 23.73 N · m maximum continuous torque
Core size	0.25 m long, 0.027 m diameter

FIG. 5. A photograph of the MARTE drill mounted on the lander.

surface-set monocrystalline diamonds were used. A full-faced carbide cutter is also used to establish an initial hole to start drilling in bedrock of unknown composition.

The core barrel located in the lead drill string can contain up to 25 cm of core. Continuous coring requires that the drill string be removed from the borehole and the core barrel be emptied after each 25 cm of drilling. A three-axis core hand-off system interfaces to the drill to accept core and place it in the CSHS core clamp. This involves positioning the core hand-off subsystem beneath the drill bit, opening the gripper, and accepting the core barrel from the lead drill segment. A plunger pushes the core out while the translation stage pulls the core barrel back at the same speed. Thus, the stratigraphy of the core sample can be maintained during core ejection.

2.3. Core Sample Handling System (CSHS)

The Core Sample Handling System (Winterholler *et al.*, 2005) is responsible for holding, moving, storing, and ejecting cores. It also obtains subsamples, crushes them to powder, and transfers powdered samples into the life-detection instrument. This subsystem, built at the University of Oklahoma, consists of several robotic devices (Fig. 6), including the core clamps, core liner feeder, linear rail and cart, core storage system, facing saw, subsampling system, crushing system, and sample transfer system. Each of these will be described briefly here; for details see Winterholler *et al.* (2005).

The CSHS receives a core from the drill into a core clamp, a 24-degree-of-freedom gripper designed to hold tightly onto a core that could be anything from a solid rod to unconsolidated rubble. Prior to receiving core, a feeder places a flex-

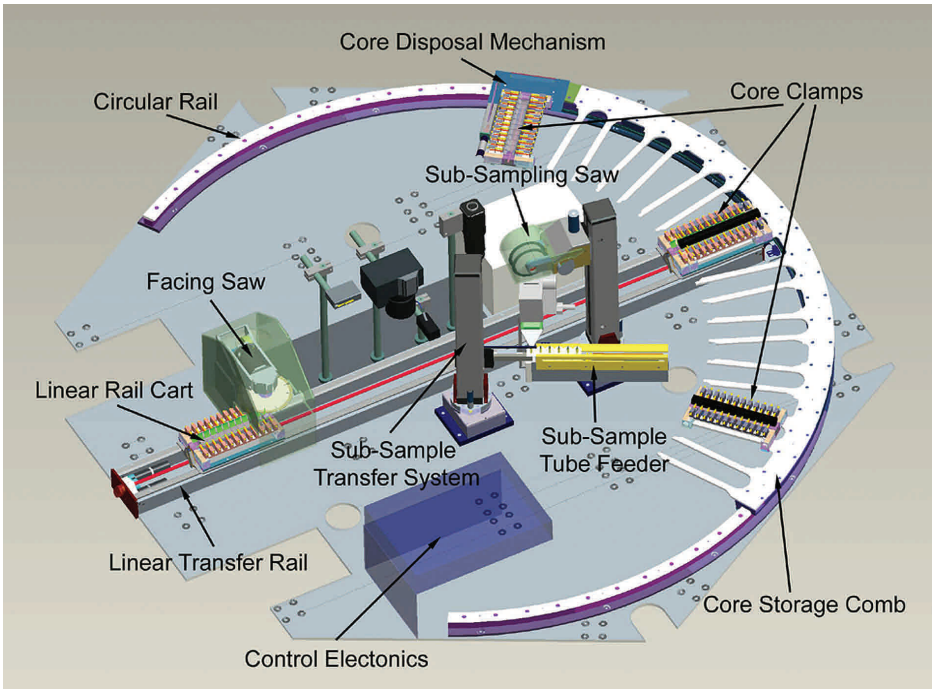

FIG. 6. CAD model of the Core Sample Handling System (CSHS) showing the location of all the subsystems.

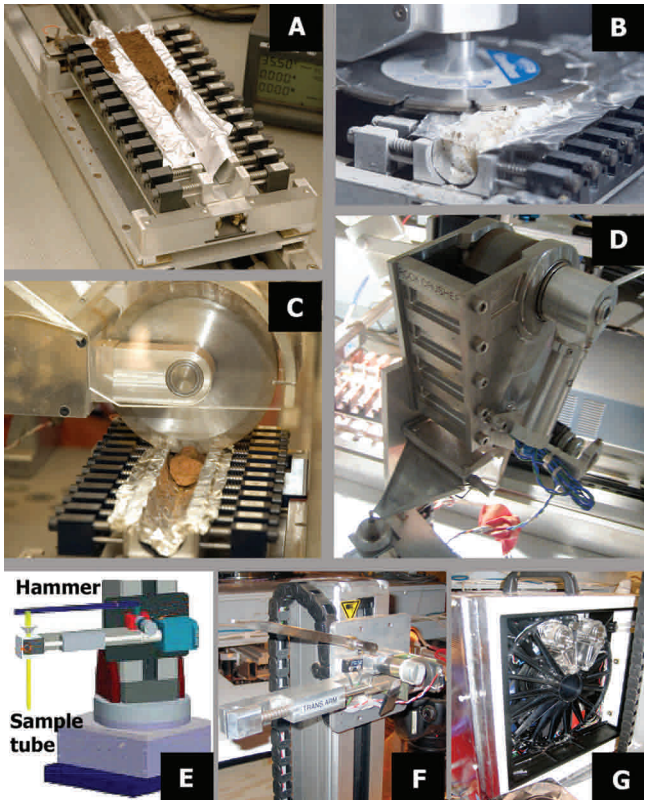

FIG. 7. Subsystems of the Core Sample Handling System (CSHS). See text for detailed functional descriptions. (**A**) Core clamp seated on linear rail; (**B**) Facing saw cutting core; (**C**) Subsampling saw; (**D**) Rock crusher; (**E**) CAD model showing the powdered-sample transfer mechanism; (**F**) Photograph of the subsample transfer mechanism. (**G**) Signs Of Life Detector 2 (SOLID2) instrument.

ible liner onto the top of the core clamp that helps contain small chips and grains in the clamp. The clamp (Fig. 7A) is composed of 12 concave-shaped, spring-loaded fingers that apply a clamping force compliant with a core's (possibly irregular) shape. Spaces between the fingers enable the subsampling system to cut through the core and remove a subsample.

The core clamp rides on a cart that is mounted on a 2 m long pair of aluminum tracks (Fig. 6). By shuttling along the rail, the core can be stopped at specific locations, and the speed at which the core moves along the rail can be precisely controlled. The core must move under the facing saw slowly enough to allow the top of the rock to be removed without binding on the saw, but movement between stations is desired to be faster to quicken overall operations. A twin motor design is used to accomplish the fast and slow motion requirements. The underside of the cart includes a mechanism to open and close the clamp and to release the clamp from the storage comb (see below).

Core clamps are stored on an assembly that includes a stationary circular rail and a rotating storage comb arranged in an arc around the edge of the DCSM (Fig. 6). Rotation of the comb uses a rack and pinion drive. Core clamps are exchanged on the storage comb by unlocking the core clamp from the linear rail cart and locking it into the core storage system. The linear rail cart is pulled out underneath while the core clamp rests on the core storage system. The storage comb has nine rigidly mounted forks and one fork that pivots at the comb frame to serve as a core ejection mechanism. To dispose of core, the opened core clamp is moved to this location where a power-screw linkage rotates the pivoted storage fork vertically. The core slides out of the clamp and falls to the ground.

After the core is placed into the clamp, it is run under a "facing saw" (Fig. 7B) that cuts open the core and produces a clean, even face to be viewed by the remote inspection instruments. Without this procedure, drill cuttings embedded in the core by the drilling process obscure its surface and prevent useful imaging. A dry diamond-encrusted masonry blade, 150 mm diameter × 2.6 mm thick, with a discontinuous circumference to allow better chip removal, is lowered into position 5 mm from the top of the core clamp. After facing, the core can be run under a suite of remote sensing instruments positioned along the linear rail. Data from these instruments are used to determine where subsamples should be acquired for analysis with an *in situ* life-detection instrument.

Subsampling is accomplished with twin saw blades of the same design as the facing saw, which are mounted on a rotational/vertical actuation base (Fig. 7C). The saw blades are lowered down perpendicular to the core and positioned on either side of the slots between clamp fingers. Once the saw has sliced through the core, the blades squeeze together to pick up the piece of rock and then are moved vertically to the level of the top of the rock crusher (Fig. 7D). The rail that holds the blades rotates around the vertical axis so that the blades swing over the entrance jaw of the rock crusher. The blades are then moved apart, and the core fragment drops into the crusher.

The rock crusher (Hansen *et al.*, 2007) works by successive fracturing of a rock sample placed between two metal plates that meet at a hinge point. A motor operates the hinge, varying the angle between the two plates. When the angle increases, gravity causes the rock to slide toward the hinge; and when the angle decreases, the rock is crushed between the plates. Crushed fragments of rock fall through a sieve at the apex of the angular plates near the hinge point, and the fine particles move into a chute. A small vibrator motor assists movement of powdered rock through the sieve.

Sample transfer from the rock crusher to the Signs Of LIfe Detector (SOLID2) instrument is accomplished by the powdered sample transfer stage (Fig. 7F, 7G) as follows: powder entering the chute pours through a small funnel at the top of a sample transfer tube that has some small fill holes. The chute touches the funnel, which causes it to vibrate, and the small rock particles stream into the funnel, through the holes, and into the tube. The tube has a plug on the bottom that can be opened by pressing on the spring-loaded stem at the top of the tube. A spring-loaded rack holds the tubes in place. The subsample transfer arm (Fig. 7E, 7F) is used to move the sample tubes from the tube array to deposit the sample into the instrument. It uses an identical rotational/vertical actuation base as the subsampler. A solenoid-actuated gripper slides open once the subsample transfer arm is moved into position to pick up a full tube. The solenoid is released, and the gripper is held closed by a return spring. The tube can then be lifted and rotated over the SOLID2 instrument. Then

Table 2. Remote Science Instruments

Instrument	*Measurement type*	*Field of view*	*Resolution*	*Data volume*	*Manufacturer*
Core Context Imager (CCI)	Color image of whole core	25 × 17 cm	125 μm/pixel	3.2 MB	Canon PowerShot S230
Microscopic Imager (MI)	Color microscopic image of core sections	2.5 × 1.7 cm	7 μm/pixel	6.7 MB	Canon EOS 10D
VNIR point spectrometer	Point spectra 400–1080 nm spectral range	5 mm spot	25 μm = 4.2 pixel	32.7 KB	Ocean Optics S2000
VNIR imaging spectrometer	Spatially resolved spectra	Full length of core	50 μm spatial, 780 spectral elements over 400–1000 nm range	239 MB	NASA Ames Research Center

the lower half of the sample tube is lowered into an opening on top of the instrument, and the hammer motor is turned on to release the contents of the tube. The motor spins a crank connected to the hammer and depresses the spring-loaded seal on the bottom of the tube.

The entire CSHS sequence of operations is performed autonomously via 18 powered actuators with sensors. To get high positional accuracy and repeatability, and maintain flexibility, a custom controller is used that is a modification of an XBC controller (LeGrand *et al*., 2005). The controller makes use of a 100K gate floating point gate array to handle the motor and gear controls along with the digital inputs from the sensors. The floating point gate array is controlled by a Nintendo Game Boy, which acts as central processor with debugging display screen connected through the game port slots.

2.4. Remote science instruments

After the core is received and faced, it rides in the core clamp along the linear rail and under a sequence of remote sensing instruments. Information received from them is used to determine core geology and select locations for subsampling. Table 2 shows a summary of the characteristics of these instruments. First, the core stops under the Core Context Imager (CCI). A single color image captures the full length of the 25 cm long core segment at a resolution of about 125 μm/pixel. The imager is a 3.2 Megapixel (2048 × 1536 pixels) Canon PowerShot S230 with functions (shutter release, zoom, flash, white balance) remotely operable via a computer interface. The largest JPEG image file generated by the camera is 1.6 MB.

Next, the core is moved under a Microscopic Imager (MI). The MI is a Canon EOS-10D digital camera with a 100 mm macro lens that obtains color images with resolution of 7 μm/pixel and a field of view of 2.5 × 1.7 cm for a file size of 6.7 MB. In our study, four images were typically obtained, which were spaced equally along the arriving core clamp.

Point spectra centered on the location of the above images are next obtained by the Visible–Near Infrared (VNIR) point spectrometer, an Ocean Optics S2000 fiber optic spectrometer with a #3 grating (range of 400 nm to 1050 nm) and a high-sensitivity linear CCD array (2048 element). The VNIR point spectrometer system includes the thermally controlled spectrometer, an A/D converter with USB computer interface, and a tungsten-halogen illumination lamp. The reflectance probe contains six illuminating and one collector fibers, all 400 μm in diameter.

The core is next scanned by the VNIR imaging spectrometer. This instrument, built at NASA Ames Research Center for the MARTE project (see Brown *et al*., 2008) obtains spatially resolved spectra of the core samples at lower spectral resolution than the VNIR point spectrometer. It uses macroscopic imaging optics and a slit input aperture to sample a line on the object (core). A combination of dispersive and diffractive elements and relay lenses provides light to the array detector, which is separated spatially along the slit in one dimension and spectrally along the other array dimension. This is sampled with an 8-bit monochrome industrial-vision CCD camera that scans the core in a direction normal to the slit while taking multiple images. This allows for the formation of a data hypercube in the mode of classic push-broom-type remote sensing instruments (*e.g*., PHILLS, HYDICE).

The VNIR imaging spectrometer resolves 580 columns of 50 μm spatial elements along the input aperture. The hypercube image length is only limited by the length of the scan, here configured for rock cores that are 25 cm long. The spectrum is sampled by 780 detector rows that span the 400–1000 nm wavelength range. These over-sampled spectral data are averaged, typically over six rows, to improve signal quality and reduce hypercube size. The VNIR imaging spectrometer operates under current-controlled tungsten-halogen illumination to permit the derivation of reflectance data. A "quick-look" color image is produced at the end of the scan, which is comprised of three wavelength bands that represent normal human perception of red (660 nm), green (530 nm), and blue (460 nm). This image is provided to the science team members, who may specify regions of interest in the quick-look image and send a request to the

onboard hypercube data mining software, which returns reflectance spectra data averaged over these regions. In the course of the remote science experiment, the hypercubes (each were 377 MB) were too large to download but were stored in the field pending requests for specific spectra by the science team. The instrument provides ~48 dB max signal-to-noise ratio, as limited by the dynamic range of the camera and particularly limited in the short- and long-wavelength regions by the spectral response of the silicon CCD sensor and the black-body intensity distribution of the tungsten-halogen lamps.

Immediately before and after each core is cut with the facing saw, the external surface of each core is tested for the presence of adenosine-5′-triphosphate (ATP) (via bioluminescence). ATP is the energy mechanism for all living organisms. In the study, we thought that an ATP assay might provide a quick-look assay for the presence of bacteria in cores either as an indication of contamination [see Miller *et al*. (2008) and Bonaccorsi *et al*. (2008)], or plausibly as a method of life detection (see Bonaccorsi *et al*., 2008). The assay was performed with a Lightning MVP portable luminometer (BioControl Systems Inc.). The Lightning MVP instrument uses a luciferin-luciferase enzyme as a reagent to react with the ATP present in the sample to emit light that is then detected by the instrument. To perform the assay in the field, a sterile cotton swab was rubbed along the surface of a core then placed into the instrument chamber where the reagent was added and the assay performed. The reagent causes fluorescence in proportion to the amount of ATP present. [See Miller *et al*. (2008) for more details on the interpretation of the ATP assay.] The reading takes about 10 seconds and is measured in relative light units (RLU). The ATP luminometer has a sensitivity of 15 picograms of ATP.

After the core is examined with the remote sensing instruments and the ATP assay is performed, the core is stored in the core rack until the science team can analyze the observations to decide where to subsample the core for *in situ* life-detection experiments using SOLID2. It is also possible to retrieve the core from the storage rack to perform further remote sensing inspections if desired.

2.5. Signs Of LIfe Detector (SOLID2)

In the study, samples were analyzed for the presence of life with the Signs Of LIfe Detector built at the Centro de Astrobiología (Parro *et al*., 2005, 2008). The instrument is described in detail in Parro *et al*. (2008) and is summarized briefly here. SOLID2 is a prototype automated flight instrument that uses protein microarray technology to detect traces of biological material in powdered or liquid samples. Only 0.5 g of powdered rock is required to perform the analysis. SOLID2 detects biochemical compounds (nucleic acids, proteins, polysaccharides, etc.) via microarrays printed with antibodies.

The instrument setup used by MARTE was sensitive to 157 different antibodies produced, with use of the strategy and methods described in Parro *et al*. (2005). Antibodies were produced against natural extracts of Río Tinto water and sediments, and microbes found in Río Tinto rocks during the ground truth drilling experiment; and commercially available antibodies were also used that produce diagnostic results.

When a compound in the sample and an antibody on the array match, a fluorescent tag is excited by a laser beam, and the array cells are imaged by a CCD camera that detects the bright spots. SOLID2 can detect chosen compounds with ppb sensitivity.

2.6. The Borehole Inspection System (BHIS)

After the core is retrieved to the surface and the drill is removed, the walls of the hole are imaged and analyzed with the Borehole Inspection System (BHIS). Figure 8 is a drawing of the BHIS showing the main components of the mechanical system. Figure 9 shows images of the BHIS during operations. Table 3 summarizes the BHIS characteristics. Built at Centro de Astrobiología, the BHIS includes two probes, the Borehole Inspection Tool (BHIT), and the Borehole Standard Probe (BHSP). The BHIT was custom built for the MARTE robotic drilling project. The BHSP is a commercial borehole logger for magnetic susceptibility, which was not used during the MARTE experiment. The BHIS has separate reels and tether support systems for the two probes (Fig. 8). The cylindrical probe (150 cm long) of the BHIT houses two cameras and the optical head of a fiber optic Raman spectrometer along with supporting electronics, three stepper motors, and two linear motors. Fiber optic and electrical wires are housed within a 25 m long tether that winds around a drum and reel mechanism. The BHIT is held stationary in the borehole with flexible rubber seals at either end of the probes' length, which deform outward when compressed and form a sidewall anchor. Using the reel and the anchoring, the BHIS can position the inspection tool from depths that range from 0 to 25 m with high precision.

The payload section of the BHIT is at the downhole end, and the optical window for collecting spectra and images is located 50 cm above the probes' end. The payload module houses light-collection and illumination optics for a boresighted fiber optic Raman spectrometer and an imager. The laser and detector elements of the Raman spectrometer are housed within the tether reel on the surface. The excitation

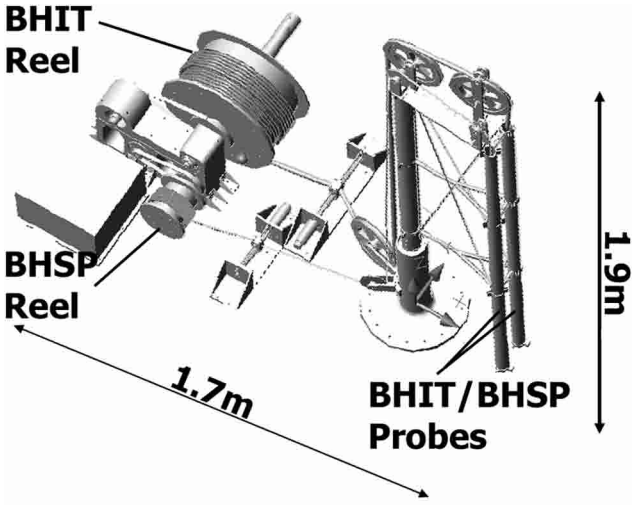

FIG. 8. CAD model of the Borehole Inspection System (BHIS) showing support structure, tether reels, cable guides, and electronics box.

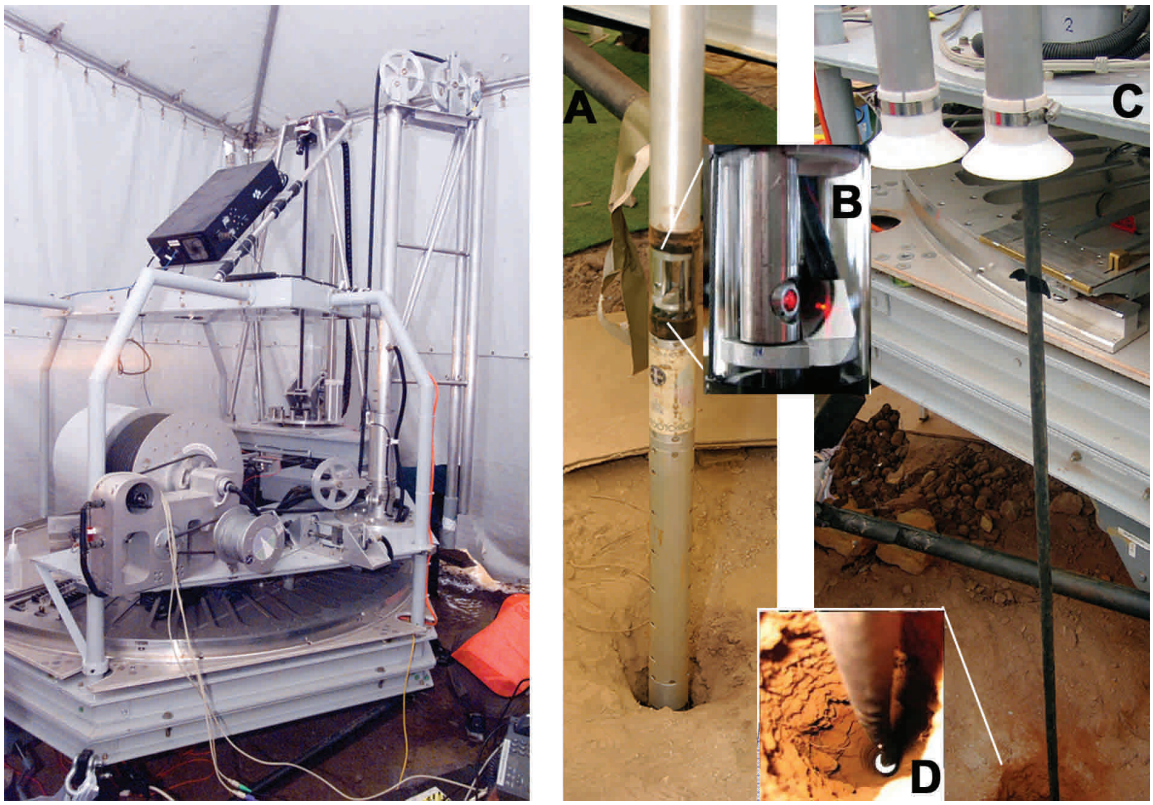

FIG. 9. Left: Picture showing the Borehole Inspection System (BHIS) structure mounted on the lander. **Right:** (**A**) Picture of the Borehole Inspection Tool (BHIT) probe deployed in the borehole. Inset (**B**) is a close-up of the optical window with the laser turned on for collection of Raman spectra. (**C**) Shows the probe tether leading into the borehole and (**D**) a view down the borehole with the tether line running to the top of the BHIT.

source of the Raman Spectrometer is a 5 mW helium-neon (He-Ne) laser coupled into fiber optics that transmit the light through the tether to the subsurface optical port. The He-Ne laser provides low noise, good beam-pointing stability, and thermal amplitude stability. The detector is a Jovin Ibon spectrometer, with response in the wavelength range 200–3600 cm^{-1} and spectral resolution of less than 10 cm^{-1} controlled by a PCI bus CCD controller board. Stimulated Raman emission is collected by downhole optics and transmitted via fiber optics to the detector.

The sensor elements, including the illumination and light-collection optics for the Raman spectrometer and the cameras, are located inside the BHIT. The processing and control electronics, the laser, and the grating and CCD detector elements of the Raman spectrometer are located on the surface inside the tether reel. Electrical wires and optical fibers in the tether link the two sections.

Figure 9 shows the BHIS mounted on the DCSM platform (left) along with a detail of the BHIT payload section with the laser on (right image). To image the walls of the hole as well as the spot analyzed by the Raman spectrometer, the BHIT uses two color CCD cameras (M820, JAI Inc.) with

TABLE 3. BHIS CHARACTERISTICS

System component	*Characteristic*
BHIT probe volume	1.5 m long, 3.8 cm diameter
BHIT probe mass	3.4 kg
BHIS deployment structure mass	98.4 kg
Operating power	20 W nominal
BHIT payload	
Camera 1	752 × 582 pixels, 25 μm/pixel
Camera 2	752 × 582 pixels, 18 μm/pixel boresight with Raman optics
Raman spectrometer	633 nm laser, spectral resolution 10 cm^{-1} in 200–3600 cm^{-1} range. Light transmitted downhole using fiber optics.

effective pixels at 752 (w) × 582 (h). One camera provides 360° imaging of the borehole walls at 25 μm/pixel resolution, and the other camera provides individual images (18 μm/pixel resolution) boresighted with the Raman spectrometer field of view. The cameras are located longitudinally through the BHIT and parallel to the Raman spectrometer head. Illumination is provided by wide-aperture white LEDs located close to the cameras. A 45° angle fold mirror, located at the optical axis of each camera, points the images at the borehole wall. Slight shifts of the cameras relative to the mirrors (up and down within the BHIT) allow the images to be focused. Panoramic imaging is accomplished by rotating the inner components of the BHIT (cameras, mirrors, and the Raman spectrometer head) around the circumference. A single panoramic image of the borehole wall is acquired by stitching together the central pixels in an image sequence using onboard image registration and stitching software. Raman spectra and boresighted images can also be collected at user-selectable points around the circumference of the borehole.

2.7. Remote operations subsystem

In this study, the remote operations subsystem provided data communications between the borehole and the science operation centers over a remote satellite link. The science team gave daily activity requests to the operations team, who translated each request into a command to the robotic system. After the request was executed, the resulting data were loaded to a server visible to the science centers. This was accomplished in a way that simulated a real mission from the scientists' perspective.

The operations engineers were located in the field with the drill, and commands were written from that location. The drill platform was automated in the sense that, once commands were uploaded to it, they were executed without human intervention, and it would have been possible to write/upload commands from a mission control site anywhere with an internet connection. However, logistics dictated putting the engineering team in the field where they could also handle any technical problems that arose.

Centralized command and data handling for controlling all the robotic systems was accomplished through an executive controller based on the Contingent Rover Language (CRL) used on previous NASA Ames robotic platforms (Bresina *et al*., 1999). Commands to each subsystem came only from this executive, and data transmitted to the mission operations center were transmitted through a telemetry server at the request of the executive. This way, subsystems only needed to communicate with the executive and the telemetry server. There were no communications between the subsystems themselves. A plan file was created by operations engineers based on the requests submitted by the science team. The executive executed the plan by sending commands to a communications package that utilized Common Object Request Brokering Architecture (CORBA) to transfer data between clients and servers. The servers cause the commands to be executed by calling appropriate routines in the subsystem control software. Since the MARTE system did not include onboard diagnostics, it was necessary at times for the human operators to detect system hardware failures and take action. To enable this capability, the CRL Executive allowed operator intervention followed by seamless continuation of plan execution.

The borehole equipment was automated to ease the overall complexity of operations and prove out automation software technologies (Cannon *et al*., 2007) for a drilling mission. Human intervention was allowed to handle faults as they occurred, to handle non-automated instrumentation (such as the ATP luminometer) and to provide non-mission-related support such as cleaning and sterilization. In particular, all mechanisms that had physical contact with potential samples to SOLID2 were kept sterile by the application of field protocols to minimize environmental and cross contamination (see Miller *et al*., 2008).

2.8. Science mission description

The remote science mission simulation took place from September 3 to September 30, 2005. Due to this long duration, and to broaden the international participation, science operations were conducted at two locations—Centro de Astrobiología in Madrid, Spain, and NASA Ames Research Center in Moffett Field, California—each of which ran for a period of two weeks. In the first period, the team in Madrid led mission operations, while the other team watched the progress via the internet. At the end of this period, a handoff teleconference was held, and the team in California assumed control for the remainder of the mission.

The objectives of the remote science mission, as provided to the science team, are listed in Table 4. The science team operated under "blind protocol," that is, they were provided only minimal information about the site location. They were told only that the mission simulation would be performed at a field site chosen for its relevance to Mars and that the site was in Southern Spain near the Río Tinto river. Some members of the Madrid science team had previously visited the site or had knowledge of the area, so we did not provide satellite or aerial imagery that might be available to a Mars mission team. In case any familiarity with site geology may have caused an interpretation bias, all science team members

Table 4. Mission Objectives

1	Obtain practical experience interpreting observations obtained from a remotely operated drill in a field site off interest as a Mars analogue.
2	Determine (by comparison with ground truth) what can be learned from the science payload on the drill and what improvements might be needed.
3	Analyze data from core using remote sensing instruments and downhole instruments to identify mineralogy, stratigraphy, indicators of aqueous activity, and indicators of biological activity.
4	Choose levels of interest on cores to conduct further *in situ* measurements on powdered subsamples to search for signatures of extant life using robotic life-detection instruments.
5	Investigate how a multinational and physically separated science team can collaborate effectively.

attempted to analyze and interpret the data "as if it came from Mars" (see Prieto-Ballesteros *et al*., 2008).

Access to the data was via a user interface specifically designed for this mission with a web-based open architecture structure (TWIKI, Huffman *et al*., 2006). The interface also provided tools for the scientists to generate daily operation requests. Each operation day, the science team was provided the data obtained during the previous day's operations; the team analyzed this data and, by the end of the day, sent a request for the next day's operations to the mission operator. Then, a teleconference was held with the mission operator to go over the command and clarify any open issues.

The normal flow of operations occurred as follows:

(1) The science team provided the operations team with a daily plan that consisted of directives covering depth to drill, borehole locations to inspect with the BHIS, core subsamples to collect and insert into SOLID2, and cores to eject. If drilling was requested, a maximum drilling depth to achieve was specified. If using the BHIS, scientists could request where in the hole to take images and Raman spectrometer measurements. When drilling was requested, scientists specified which currently stored cores to keep and which to eject, since a maximum of only 9 cores could be stored in the CSHS at any one time. As each core came out of the borehole, it was inspected with the RSI instruments in a pipeline process. However, the scientists could request additional measurements if there were problems with the data or as desired.
(2) The mission operations lead examined the plan to determine whether it was feasible given the status and capabilities of the equipment. If there were any problems, the plan was rejected and follow-up discussions occurred via teleconference to negotiate a plan that could be accomplished in a day.
(3) After accepting the plan, the mission operators translated it into machine commands that were executed via the onboard automation equipment.
(4) After execution, the resulting data were uploaded to a server and made available to the science team via a science data browser accessed through a web interface.
(5) After examining the data, the science team planned the next day's activities.

3. Mission Results

Here, we discuss the mission performance and key results. Table 5 shows the predefined criteria for mission success. All were achieved during the simulation. Under science team direction, a depth of 5.7 m was drilled with accompanying core analysis, interpretation, and selection of locations for SOLID2 analysis. All the instrumentation, systems, and modes of operation were exercised, and valuable lessons were learned pertinent to future missions that involve drilling and searching for life. Table 6 shows a summary of the mission activities and data acquired during each day of the simulation.

3.1. Performance of the drill and sample handling system

During 21 days of mission operation, 43.1 hours were spent drilling, and the total depth reached was 6.1 m. Under science team direction, 5.7 m were drilled. The average

Table 5. Mission Success Criteria for MARTE Drilling Mission Simulation

Minimum mission success	*Actual accomplishment*
1 Drill to at least 2 m over the mission duration.	Drilled to 5.7 m over the mission duration.
2 Deploy the BHIS to its operating depth and demonstrate the panoramic imaging, Raman spectrometer, and microscopic imaging.	BHIS data collected in 16 sections of borehole. Continuous panoramic imaging obtained from 600–1200 cm.
3 Demonstrate a full operational sequence including drill, recover core, plane face of core with facing saw, collect data with RSI, swab for ATP, select subsample locations, and collect subsamples on at least 4 cores.	Full operational sequence including drill recover core, plane face of core with facing saw, collect data with RSI, swab for ATP, select subsample locations, and collect subsamples on 16 cores.
4 Deliver uncontaminated samples to SOLID2 for analysis.	15 uncontaminated samples delivered to SOLID2 for analysis.
5 Perform at least 3 life-detection analyses on cores obtained from the surface and at depth.	15 SOLID2 analyses performed from cores ranging from 750–5500 cm.
6 The science team interprets the data obtained from drilling, and results are compared to ground truth.	Data interpretations compare well with ground truth.
7 Successfully direct drilling and sampling operations from a remote site.	21 days of mission operation directed by science team.
8 Perform 2 continuous days of automated operations "hands off" at the borehole.	"Hands off" continuous drilling achieved in upper section of borehole.

TABLE 6. SUMMARY OF DAILY MISSION ACTIVITIES AND DATA ACQUIRED

				RSI data						BHIS				SOLID			
Mission day	*Date*	*Depth drilled (cm)*	*Drill end depth (cm)*	*Core #*	*CCI*	*MI*	*VNIR point spectrometer*	*VNIR imaging spectrometer*	*ATP*	*Imaging spectra retrieved*	*BHIS pan*	*BHIS Raman*	*BHIS micro*	*Subsamples acquired*	*Result images*	*Cores ejected*	*Main activities*
1	8/30	20.0	20	Pilot													Drilling starts
2	8/31	22.0	42	**1**	1	4	4	1	2								
3	9/1	22.0	65	**2**	1	4	4	1	2								
4	9/2	22.0	87	**3**	1	4	4	1			5	6	6				BHIS: Test and calibration
5	9/5	11.6	98	**4**	1	4	4	1	2								
		21.1	119	**5**	1	4	4	1	2								
6	9/6	18.2	137	**6**	1	4	4	1	2					C3-P8*		1,2	
				3		4				1							
7	9/7	9.5	147	**7**	1	4	4	1	2		6	32	32				BHIS depth: 60–72 cm
8	9/8	21.2	168	**8**	1	4	4	1	2							4, 6	
		3.5	172	**9**	1	4	4	1									
				3	1	3											Post subsampling imaging or cores made standard
9	9/9	22.0	194	**10**	1	4	4	1			7	32	32				BHIS depth: 74–86 cm
		23.1	217	**11**	1	4	4	1	2								
				3						5							
				5	1	3								C5-P7			
				7	1	3								C7-P9			
10	9/12	22.0	239	**12**	1	4	4	1	2						C3-P8	8,9	
				10	1	4								C10-P8			
				1–8						16							Remeasured to correct earlier reporting errors
											7	32	32				BHIS depth: 86–98 cm
11	9/13	31.0	270	**13**	1	4	4	1	2								
		47.5	318	**14**	1	4	4	1	2								
		6.6	325	**15**	1	4	4	1	2								
12	9/14	3.7	329	16					2						C5-P8, C7-P10, C10-P8		
				11	1	3								C11-P8			
				13	1	3								C13-P11			
13	9/15	3.0	332	**17**	1	4	4	1	2							3, 10, 13, 14	

14	9/16	3.3	336	**18**	1	4	4	1	2					C11-P8		
		19.9	356	**19**	1	4	4	1	2						C13-P9	11, 12, 15, 16
					15	1	3								C15-P9	
				16	1	3								C16-P9		
											10	20	20			BHIS depth: 130–270 cm
15	9/19	8.9	365	**20**	1	4	4	1	2							
		26.0	391	**21**	1	4	4	1	2							
		24.6	414	**22**	1	4	4	1	2							
16	9/20	24.4	438	**23**	1	4	4	1	2							
				19	1	4	4	1								Reprocessed due to original data errors
				19	1	3								C19-P9		17, 18, 20
17	9/21			19						1						
				21	2	6								C21-P7	C11-P8	
				22										C22-P9	C13-P9	
				23	1	4	4	1								
											24	24	24			BHIS depth: 225–350 cm
18	9/22	21.4	460	**24**	1	4	4	1	2							19, 22
				23						1						
19	9/23	11.9	507	**25**	1	4	4	1	2							
					1	3								C24-P9		
		55.3	509	**26**	1	1	4	4	1	2						
20	9/26			25	1	3				4				C25-P8, C25-P10	C24-P9	
		30.3	558	**27**	1	4	4	1	2		4	16	16			BHIS depth: 268–273 cm
21	9/27	19.7	557	**28**	1	4	4	1	2							
											5	20	20			BHIS depth: 405–411 cm
22	9/28				1	3				7				C23-P5	C25	
					1	3								C23-P9		
														C27-P9		
23	9/30										6	24	24		C19, C22, C23, C24	BHIS depth: 458–510 cm

*Designation C = core P = clamp position; C3-P8 means core 3 position 8.

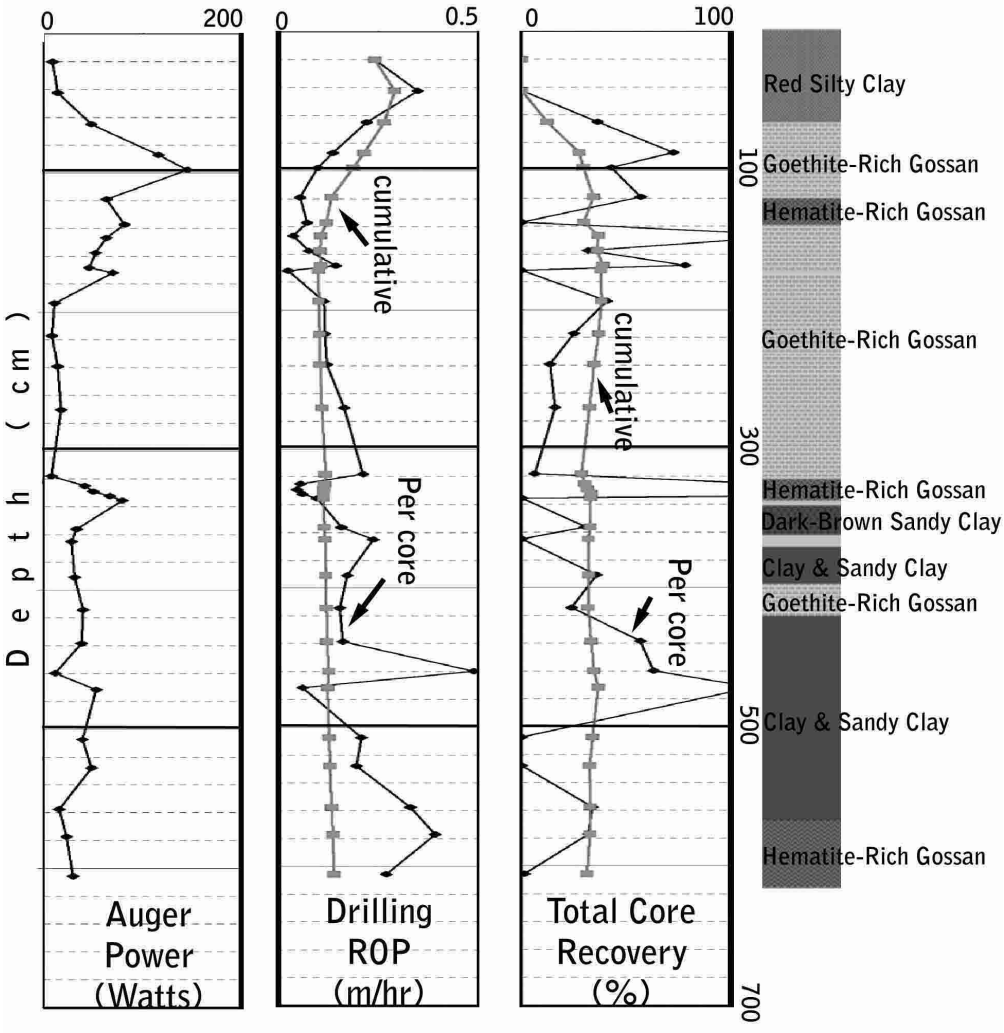

FIG. 10. Drilling performance as a function of depth. Left to right: auger power, penetration rate, and core recovery.

penetration rate while drilling was 0.14 meters per hour. Figure 10 shows the rate of penetration (ROP), auger power, and core recovery as functions of depth. Table 7 shows relevant drill performance information. The core recovery was relatively low: 32% averaged over the entire depth. The material drilled was heterogeneous and largely unconsolidated (Fig. 11), which resulted in core loss from the core capture mechanism.

During the mission, bit changes and the use of an air jet to move cuttings were attempted to improve rate of penetration and core recovery and prevent the drill from stalling. Three different arrangements of diamonds on bit heads were used, and a carbide bit was used to drill more unconsolidated material. Automated bit change-out was not part of the design, so changing bits required a manual procedure. The first 17.5 cm was drilled with a larger-diameter carbide starter bit to make a guide hole for the coring operation. We then changed to the diamond coring bit, and performance was good until 97 cm below the surface, when the ROP dropped dramatically. At a depth of approximately 160 cm, the drill became stuck, as indicated by a rapid increase in auger torque, and was pulled out of the hole and cleared manually. Upon reinsertion, it became stuck again, and cuttings removal with compressed air was started. This continued until a depth of 318 cm was reached, when a layer of fine-grained material was encountered, and the air jet appeared to be preventing core recovery by blowing the fines out of the core barrel. Air use was discontinued from 318.3 cm to 335.6 cm. Penetration rates were quite low, however, so air use was resumed. By this time, core recovery was adequate to satisfy the primary science mission objectives, and the drill team wanted to increase drilling rate to achieve maximum depth as a technical milestone, whereas the science team wanted to capture core. A compromise approach was adopted to obtain some core in each drilling cycle for science analysis, while also achieving better penetration rate. From 335–600 cm depth, air was turned on for the first interval of 10–20 cm and then shut off for an additional 10–20 cm interval. This resulted in core recovery at every drilling cycle.

The relatively poor core recovery in unconsolidated material could be improved by redesigning the core capture system, since no direct means to prevent the unconsolidated core from falling out of the end existed. The design depended on two small keys and friction to lock the core in place. A simple design change should be implemented to prevent core loss from the core tube.

TABLE 7. DRILL PERFORMANCE

Day	*Date*	*Bit*	*Core #*	*Approx. drilling duration (s)*	*Depth drilled (cm)*	*Core length (cm)*	*Avg. auger power (W)*	*Approx. drilling ROP (m/hr)*	*Bit condition/recovery notes*
1	8/29	Starter	Pilot hole	3000	20.02	0	8.6	0.24	Lots of wear and chipping
2	8/31	SSD #1	1	2300	22.00	0	14.0	0.34	Several diamonds missing and several dulled
3	9/1	SSD #1	2	3600	22.00	8	47.5	0.22	No change in wear, pebbles
4	9/2	SSD #2	3	5750	22.00	16	114.8	0.14	Bit OK, not much wear
5	9/5	SSD #2	4	4150	11.63	5	143.3	0.10	Pebbles, big and small
		Carbide	5	13000	21.05	12	62.7	0.06	
6	9/6	Carbide	6	8600	18.20	0	80.5	0.08	
7	9/7	SSD #2	7	8120	9.52	12.7	62.3	0.04	Hit competent layer at end (retained core)
8	9/8	SSD #2	8A	4800	10.68	3.4	51.6	0.08	Competent layer at beginning (pushed unconsolidated material out)
		SSD #2	8B	2600	10.49	8.23	45.3	0.15	Got stuck at the very end . . . core mostly powder
		SSD #2	9	4200	3.45	0	69.0	0.03	Got stuck very fast (modified bit beforehand)
9	9/9	Carbide	10	6800	22.00	9	10.7	0.12	Solid rock pieces—compressed air used
		Carbide	11	7000	23.11	5.8	7.9	0.12	
10	9/12	Carbide	12	6400	22.00	3	13.7	0.12	Solid rock pieces—compressed air used
11	9/13	SSD #0	13	6750	31.00	5	17.1	0.17	Solid rock pieces—compressed air used
		SSD #0	14	8100	47.51	3	7.5	0.21	
		SSD #0	15	4000	6.63	7.6	41.0	0.06	Packed clay core
12	9/14	SSD #0	16	2650	3.72	5	49.3	0.05	Packed clay core
13	9/15	Carbide	17	1675	2.97	7	66.0	0.06	
14	9/16	Carbide	18	1180	3.28	0	78.6	0.10	Low recovery due to vibration of bit during 60 rpm drilling
		SSD #0	19	4500	19.90	6.1	32.6	0.16	Air at 10 psi, shut off at 15 cm
15	9/19	SSD #0	20	1350	8.88	0	27.7	0.24	Air at 10 psi, turned down at about 8 cm (got stuck)
		SSD #0	21	5400	25.95	9.3	30.8	0.17	
		SSD #0	22	5700	24.57	5.9	39.0	0.16	
16	9/20	SSD #0	23	5400	24.40	13.9	37.5	0.16	Air at 25 psi, shut off at 20 cm
17	9/22	SSD #0	24	1600	21.36	13.5	11.1	0.48	Air at 25 psi, stalled at 21 cm with air
18	9/23	SSD #2	25	6600	11.90	13.2	52.3	0.06	Air at 25 psi, 0 ROP at 11.9 cm with air
		SSD #2	26	6300	36.29	0	38.6	0.21	Air at 25 psi, stalled at 36.29 cm with air
		SSD #2	26	3500	19.05	0	47.5	0.20	Air at 25 psi until 5273.23 mm then shut off air
19	9/26	SSD #2	27	3340	30.30	10.3	15.3	0.33	Air at 25 psi until 21 cm then shut off air
20	9/27	SSD #2	28	1830	19.67	6.3	22.5	0.39	Air at 25 psi until 15 cm then shut off air
21	9/30	SSD #2	29	4800	35.74	0.5	29.1	0.27	Air at 25 psi until 30 cm then shut off air

A number of design changes should be considered to improve drill performance. The capture of a continuous core substantially limited drilling performance because a lot of time was required to retrieve the core barrel from the hole, especially at deeper depths. A potential optimization of the coring approach would be to use selective coring instead of continuous coring. During the design phase, we decided that we wanted a complete core record for scientific analysis. However, this required that the drill be retrieved after every 25 cm in case the core barrel filled up. In a scenario such as this, the drilling process is suspended for a significant period every time a core is retrieved, and every operation in the process (core break, drill segment attach/detach, core transfer) represents a potential failure mode. To minimize this, an alternative strategy could be to selectively decide when to take a core. Then the drill bit could stay in the ground longer to make faster progress in subsurface penetration.

Another improvement to consider is the use of fluids to remove cuttings. In most cases, we flushed cuttings with air to speed things up, but there were times when it may have been mission critical to use fluids to avoid getting the drill stuck. While it is plausible that a tank of compressed gas could be included in a drilling mission, this would be a consumable that could limit drilling activities. Zacny *et al*. (2004) showed that, when drilling icy materials under martian pressure and temperature conditions, the heat of drilling leads to rapid evaporation of the ice, forming a jet of expanding gas that removed cuttings. Optimizing the design of the augering system may also improve cuttings transport. Further work to improve cuttings transport is a valuable direction for research and development for extraterrestrial drilling.

FIG. 11. Examples of core material recovered from the drilling. Each panel is an image of the material recovered from the borehole taken in the core clamp by the Core Context Imager (CCI). Left to right are Cores 3, 5, 7, 15, 23, 25, and 28. See Table 6 for depths and other drilling information associated with these cores.

The core clamp, facing saw, and subsampling system mechanisms functioned remarkably well. Given that the CSHS was a completely new design and nothing like it had ever been built before, its performance was excellent. However, the facing and subsample saws generate a lot of rock dust that could coat the lander deck, contaminate instrument ports, and possibly foul the linear rail supporting the core clamp. In our study, a dust-containment vacuum system was installed to prevent the accumulation of dust in critical areas and aspire cuttings dust (Miller *et al.*, 2008), but the power and airflow requirements of such a system would be problematical for a flight mission, especially in the thin atmosphere of Mars. Further work is needed to design a dust-containment system for drilling in situations with little or no atmosphere.

3.2. Science mission results and comparison of observations with ground truth

The science team commanded drill operations for 21 days, using all the instrumentation to develop an understanding of the geology and biology at the site. The science analysis was focused by the operational need to determine the best place to extract subsamples for SOLID2 analysis and to perform the subsampling procedures before the core storage slots filled up and cores had to be discarded. SOLID2 could accept a maximum of 18 samples, so we expected that some cores would be rejected without sampling. Criteria used to select subsamples included indications of alteration by liquid water, evidence of organic matter or life, and microenvironments, such as cavities, where water may have produced alteration. Rapid analysis and decision making was needed to keep mission activity flowing productively, as would be true in an actual mission. Science data requests had to be provided to the field team by daily deadlines.

To aid analysis, the science team incorporated their observations into a graphical core log (Fig. 12) that included icons showing the locations of features identified as pyrite casts, rims, boytroidal texture, cavities, biofeatures, and indications of suspected lithology. The log served as a map of locations where core, BHIS, and SOLID2 analysis occurred.

3.2.1. Imaging science and interpretations. The instruments that proved most useful for interpretation of lithology and selection of sampling locations were the CCI and MI (Table 2). The CCI images provided context for other measurements and were used to determine overall core recovery, morphology, and texture of samples, and to locate positions on the core clamp fingers for subsampling locations. However, resolution of the CCI was insufficient for understanding lithology. Though it did not provide continuous coverage of the cores, the MI was needed for interpretations of lithology and was critical for recognizing alteration and diagenesis. Figure 13 shows a typical image from the MI.

From image interpretation (see Prieto-Ballesteros *et al.*,

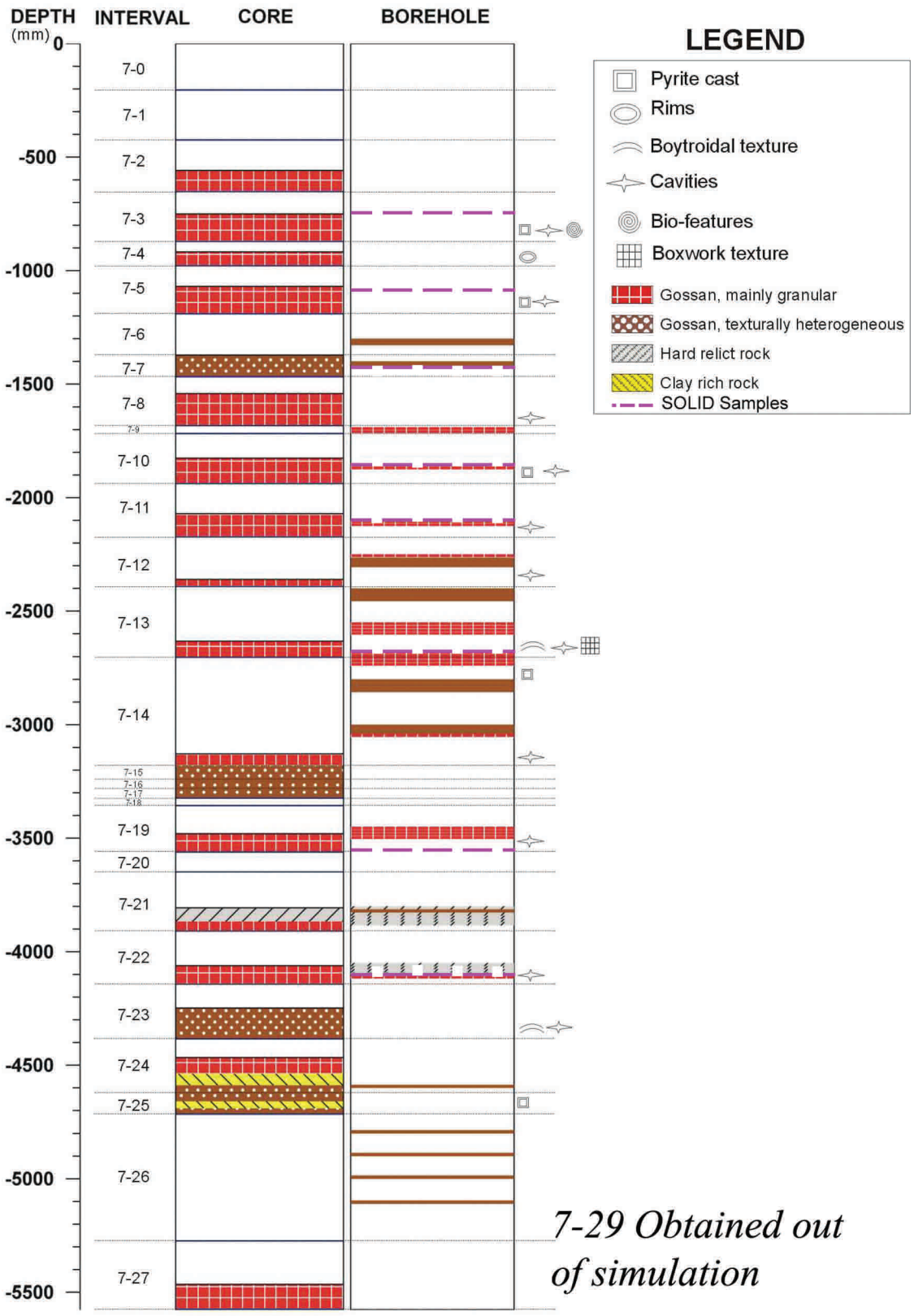

FIG. 12. The graphical core log used by the science team to organize analyses.

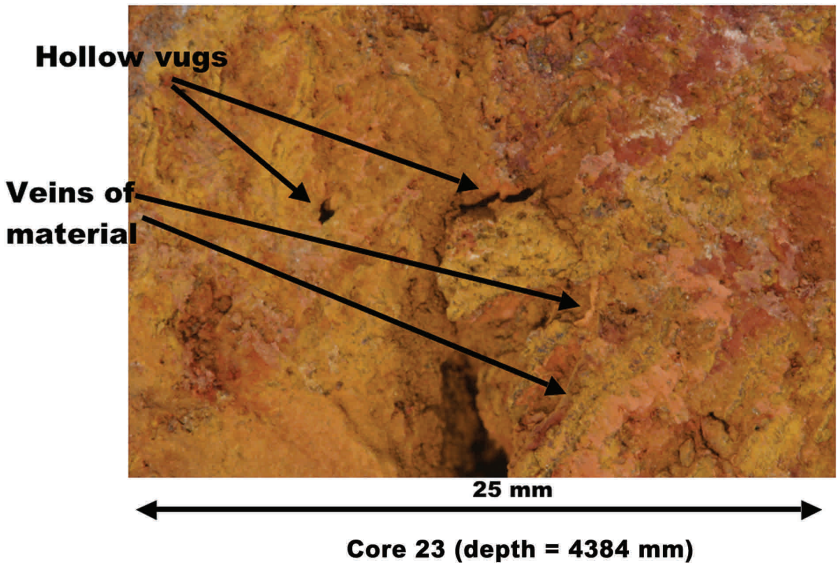

FIG. 13. Example of an image of the core obtained with the Microscopic Imager (MI). Features that led to the gossan interpretation of the lithology include the color of materials, the presence of vugs and veins, and small grey grains interpreted to be remnant pyrite.

2008), the science team concluded that the lithology was rather compositionally homogeneous and the recovered material was intensely weathered and oxidized, and often fragmented. Some MI images showed areas where the primary mineral had been dissolved, which left small cavities coated with iron oxides and oxyhydroxides such as hematite and goethite. Crystals of primary mineral were inferred to have been replaced by pseudomorphs. These typically had boxwork and botryoidal textures. On the basis of the composition of remaining minerals and the morphology of the cavities, the science team correctly interpreted the formation to be a typical gossan where the primary mineral (now almost or completely altered) consisted of sulfides. Thus, the inferred geologic history of the deposit began with the hydrothermal deposition of iron sulfides. The iron sulfides were later oxidized and altered by aqueous alteration due to groundwater-rock interactions. Furthermore, the stratigraphy implied a weathering profile where the upper zones were composed of more incompetent fines and lower zones of more competent rock. These interpretations were entirely correct and, while not surprising at this field site, evidence of similar processes occurring on Mars would constitute important discoveries.

3.2.2. Results from spectral data interpretation. Data from the VNIR point spectrometer (Table 2) were used to assess iron mineralogy. The oxidation state and stability of iron minerals were, in turn, used as an indicator of environmental conditions during their formation. Spectral signatures for goethite and hematite were identified (Sutter *et al*., 2008), which corroborated the interpretations based on color imaging for the presence of these minerals. Due to its wavelength range, a wider variety of mineralogy could not be assessed with this instrument.

Analysis of imaging spectra of MARTE cores is reported in Brown *et al*. (2008). Interpreting data from a hyperspectral imager with near-microscopic spatial resolution required the development of new methods to extract information from the large full-core data files. Data were used to identify Fe-bearing minerals such as goethite and hematite, and also to identify areas free of Fe-bearing minerals. Using an absorption band mapping technique in a software suite called MR PRISM (Brown *et al*., 2006), we were able to produce mineral maps of parts of three cores, as well as absorption band maps that displayed the presence of highly crystalline goethite. In a martian drilling scenario, these maps would provide valuable mineralogical context for the subsurface biological assays.

The above interpretations of mineralogy based on the spectral data were corroborated by both field observations and subsequent analysis of core samples by way of X-ray diffractometry (see Bonaccorsi *et al*., 2008).

3.2.3. Results from the ATP luminometry assay. ATP luminometry assays were performed to determine whether this method would be useful as a quick assay of life signatures. Previous results of work in the Río Tinto ground truth drilling campaign suggest that areas where subsurface life was found with other methods also showed a substantial ATP signature, at least in rock that occurred below the water table. It was hoped that a swab of the full length of each core might indicate whether a more-detailed life-detection analysis (SOLID2) should be performed. However, results show that the ATP luminometry assay was of marginal use in this regard. Even cores that contained evidence of plant matter (small woody roots visible in microscopic images) did not yield a statistically significant ATP result by way of the full core swab method. However, when an observer in the field performed a guided ATP analysis on specific areas where biological objects such as larger rootlets were seen, significantly higher RLU counts were obtained than for the overall rock. This indicates that some other evidence (such as imaging, or direct observation of spots of scientific interest) had to be used to guide the selection of targets for ATP analysis.

3.2.4. Borehole Inspection System results. Given the core loss, use of BHIS imaging to inspect the borehole and fill in knowledge gaps was highly desirable. Color differences, preferred mineral orientations, vestiges of original unweathered

rock, and variations in hardness as indicated by scratch marks from the drill in the borehole wall contributed to the analysis (see Prieto-Ballesteros *et al*., 2008). Interpretation of imaging data from the BHIS was complicated by several factors. First, the panoramic mode of the camera was not adequately illuminated for the dark rock of the borehole walls. Testing the BHIS in advance was problematical, since it required a 1 m deep hole for deployment. The illumination problem was thus only discovered after the field experiment was underway and required that the (better illuminated) microscopic imager be reprogrammed in the field to operate in the panoramic mode. Color contrast on this imager was still rather poor, due probably to still-inadequate illumination. BHIS images show relatively uniform rock throughout the depths imaged. Lithological differences in the borehole walls were subtle. It is possible that resolution of the imager was not adequate to resolve much of what was observed in the cores. The BHIS imager had a spatial resolution of ~20 μm/pixel, but understanding of the core lithology required the even-higher-resolution imaging provided by the MI (7 μm/pixel) to make out details that led to lithological interpretations. However, another factor in the apparent uniformity of the borehole walls may be residual cuttings from the drilling coating the walls. Upon ejection from the drill, the cores are covered with firmly adhered fine cuttings particles that obscure their surfaces. Removing these was a primary reason for incorporating the facing saw in the CSHS. While these factors may have obscured some available information, no clear features such as stratification or fractionation pattern were detected along the borehole wall. In most cases, it was not possible to use borehole imaging to locate where the core loss occurred in a particular interval or to correlate the core with the borehole wall.

Raman spectra were obtained for 2–4 positions azimuthally at each depth where Raman spectroscopy was requested. However, the results suggest that the Raman spectrometer may have been properly focused on the borehole wall only occasionally, because a clear Raman signature is found in only a few instances. The depth of focus of the Raman instrument with the chosen optics was small, and the borehole walls were quite uneven. The borehole diameter variation is probably due to the rubbly nature of the material drilled (Fig. 12), and multiple trips into the borehole by the drill probably progressively widened the hole. The BHIS instrument was designed assuming smooth walls and a constant hole diameter. In those occasions where good signal occurred, there is a clear indication of organics in the data; this was confirmed with follow-up laboratory analysis of the core samples from the corresponding borehole depth (Bonaccorsi *et al*., 2008). This remote detection of organics by Raman spectroscopy makes it a desirable active sensing instrument for chemical composition to enlist in the search for life. Minor design changes to the BHIS could provide larger depth of focus or variable focus to improve instrument performance.

3.2.5. Results of SOLID2 analysis. The results of the SOLID2 experiment are described in detail in Parro *et al*. (2008). Some highlights are summarized here. The SOLID2 instrument was successful at identifying life signatures, and some of these were recognized by the remote science team (RST). SOLID2 analysis was performed on 15 core samples from depths that ranged from near the surface (Core 3, 650–850 cm interval) to the deepest depth drilled (Core 27, 5274–5577 cm). Raw images from the SOLID2 CCD camera, which contained information as to where antibodies were detected, were provided to the RST for analysis; but as the team was not familiar with the details of the instrument, their analysis was necessarily preliminary. Also, the RST only obtained and analyzed SOLID2 data down to Core 9. Their preliminary interpretation identified life signatures in Cores 3, 5, and 7. To test whether the identification was correct, they requested a control experiment for Core 3 in which the sample was first sterilized by baking at a temperature high enough to destroy most biological molecules. As expected, the positive signature disappeared in the baked control (see Parro *et al*., 2008). More extensive analysis by the SOLID2 instrument team (Parro *et al*., 2008), which involved comparing results with those of laboratory control experiments, showed that various biosignatures were detected in 12 samples from Cores 3, 5, 10, 11, 13, 22, 23, 24, and 25, representing a depth range from shallow (0.6 m) to deep (4.6 m) samples. Compounds identified range from those commonly found in many living systems, such as c-AMP (cyclic nucleotides) and steroids structurally related to cortisol, to signatures of specific bacteria, including *Leptospirillum ferrooxidans*, *Acidothiobacillus ferroxidans*, and *Acidithiobacillus thiooxidans*—all bacteria known to occur at Río Tinto.

In summary, the remote drilling mission successfully demonstrated the drilling, sample handling, and science interpretation aspects of a drilling mission to Mars. This is the first time a fully automated and remote drilling and sample analysis operation has been performed. All the mission objectives were met or exceeded. The RST's interpretation of the lithology and geological history was correct as compared to ground truth. In spite of some instrument problems, and the relative unfamiliarity of the scientists with many of the instruments, all the instruments were successfully used and contributed to the interpretations. Finally, subsurface life was correctly identified by the SOLID2 instrument, and subsets of results were correctly interpreted by the RST.

4. Discussion and Lessons Learned

The results of the mission simulation were fully successful and met or exceeded all the predefined criteria for mission success. A simulation in a full mission framework brings to light the many problems and challenges encountered in an actual drilling mission and, therefore, offers guidance for improvements as discussed in this section.

The drill was optimized for sampling in hard consolidated rock. The core capture mechanism did not work well in highly weathered and unconsolidated material. This could be corrected by developing a core capture mechanism that prevents loose material from escaping.

During the field experiment, many attempts were made to improve ROP and core return and to improve the efficiency of chip removal from the bit. These included changing bits, modifying bits, changing drilling parameters through software controls (*e.g*., rpm, weight on bit), and experimenting with an air jet as a lubricating fluid. As the air jet was not performed under martian conditions, it is not relevant for a flight mission per se. However, cuttings transport by way of compressed gas could plausibly be used on

a planetary surface, and further development and testing is needed to evaluate this approach. In particular, fluid movement of cuttings will behave differently when gravity and atmospheric density are different. Future work should also include changes in bit design to improve the chip removal and transport of material. An optimal system for drilling in the unknown martian environment would include the capability for bit change-out with a range of bits provided for drilling different material types.

The time required to drill, recover cores, obtain remote sensing data, select sample sites, subsample and grind the samples, and process them by SOLID2 was significantly longer than originally predicted. Part of this was due to inevitable problems that occur in a field test, but accomplishing a mission with this level of complexity would probably require at least several months of mission time, and this duration is prohibitive for a field test. Results of this experiment suggest that a 10 m drilling mission is feasible to accomplish in 3 months' time, but a more detailed analysis of spacecraft resources would be required to verify this. Drill penetration rate could be improved by eliminating continuous coring. However, as evidenced by the incredible longevity of the Mars Exploration Rovers, a mission lifetime of 6 or more months can be achieved on a solar-powered mission.

Contamination control is a significant issue that will need to be addressed on future missions. Originally, we considered this to be primarily a problem for the experiment but not for a real Mars mission, because the experiment had numerous sources of contamination not found on Mars (see Miller *et al*., 2008). So, during the experiment, we spent a lot of hands-on effort ensuring the equipment was clean and sterilized prior to coming into contact with core samples. However, the tests also pointed out that many of the CSHS operations generated dust, which could cause cross-contamination between samples. Most of the dust resulted from the sawing operations, but the crusher also produced more dust than expected. Better methods are needed to contain and dispose of dust generated by the core processing systems. Likewise, the devices need to be refined to eliminate dust traps (*e.g*., corners) that would cause cross contamination and could possibly foul the mechanism. Air flush of cuttings was also a significant source of both contamination and cross contamination since the cuttings blown out of the hole were suspended in and settled out of the air onto all the surfaces of the drill.

The BHIS optical window was 50 cm higher than the bottom of the hole, and focusing the device required side wall anchors to be in place so that a hole depth of 1 m was needed before the BHIS could be used. In addition, the 50 cm offset of optics from core depth meant that BHIS data from the same depth interval as a core was received 2 or more days later than that core. Given the tight schedule of the mission, the BHIS was of limited utility for data interpretations that led to sample site selection for SOLID2. Still, the value of downhole observations was strongly endorsed by the science team. We recommend that future designs of such instruments put downhole optics close to the deepest end of the instrument.

The BHIT included a Raman spectrometer with boresighted images. The Raman element was the only organic detection method on the mission; and, unfortunately, it worked only sporadically in the borehole, as wall roughness often resulted in improperly focused measurements. Because of the high value of Raman spectroscopy for both mineral identification and organic detection and the need for precise spatial registration of information for sample selection, Raman spectroscopy would be valuable as a core inspection instrument. We recommend improving the depth of focus in the BHIT to accommodate more highly variable conditions. An important step to improve the performance of a BHIS imaging system will be to make the image capture system as robust and reliable as possible so as to be effective under adverse situations (such as with minimal light, variable albedo of the material imaged, bumpy texture). Significant effort was expended during the mission simulation to get the images properly illuminated and in focus. A downhole probe for imaging and Raman spectroscopy must have an efficient illumination system together with the capability to get the images and spectra into focus autonomously.

The core imaging systems on the lander were fixed focus, and core material was sometimes out of focus. Changing focus in steps would be desirable to get the complete core, including rubble, into focus. Most useful for analyzing core lithology was the core MI; but only sections of the cores were imaged, and these were not selectable by users. It would be preferable to image the entire cores at MI resolution (7 μm/pixel) so that no important mineral signatures are missed. The naturally broken ends produced by the core break-off mechanism could not be imaged with our system, and a naturally cleaved mineral face would be useful for examining the rock. Consideration should be given to finding a way to image the broken face of the core.

The core sampling system was optimized to work only on solid core and not on unconsolidated or poorly consolidated material (*e.g*., clay layers), so in all cases that was the material sampled. However, the most-degraded and most-weathered material might be of greatest interest from a life-search standpoint, so a sampling system that can handle unconsolidated as well as solid cores would be desirable.

5. Conclusions

The MARTE Mars drilling mission simulation provided insight into science instruments and drilling and sample handling technologies needed for a future mission to Mars to search for life. Drilling may be crucial to discovering whether life ever existed, or even perhaps exists today, in the subsurface of the planet Mars. The MARTE robotic drilling project has helped to advance the technology needed to perform a search for life on Mars. We performed a month-long mission simulation where a team of remote scientists directed the operation of automated drilling, core processing, and life-detection instruments, and analyzed the resulting science data. The drill reached over 6 m of depth, and 29 cores were extracted from the ground and examined by the remote sensing instrumentation, which generated 665.7 MB of scientific data, excluding the hyperspectral imager data. This represents the realistic downlink of mission data from our selected instrumentation. The hyperspectral imager created 10.9 GB of data that were subsequently used for analysis and to develop data mining techniques for hyperspectral microscopy. Using all the remote sensing information, the science team was able to identify the geologic nature of the site, interpret

the mineralogy, and select core locations for SOLID2 experiments that resulted in successful detection of biological signatures. This demonstration and the lessons learned from it will help to pave the way for future Mars drilling missions.

The scientific community has recognized the importance of drilling and has called for it in the MEPAG strategic plan and the Astrobiology Roadmap (Des Marais *et al*., 2003). However, robotic drilling technology is still in a relatively early state of development. The MARTE robotic drilling experiment has substantially advanced the state of the readiness and the understanding of the possible outcome of a Mars drilling mission. A 10 m drilling mission to Mars is a feasible goal for the next generation of Mars landed missions, but further technology development and testing will be needed before a reliable system with this capability can be flown. Given the high scientific priority, NASA should invest consistently in subsurface access technology over the next decade to ensure that a capable system will exist to support life-detection missions.

Acknowledgments

MARTE was funded by the NASA Astrobiology Science and Technology for Exploring Planets (ASTEP) program through NRA 02-OSS-01. Spanish participation in MARTE was funded by the Centro de Astrobiología. We are especially grateful to NASA ASTEP program manager Dr. Michael Meyer and CAB Director Dr. Juan Pérez-Mercader for strongly supporting the project.

We gratefully acknowledge the hard work and camaraderie from the many individuals who participated in the MARTE project, for their contributions to the development of the MARTE drilling system and their support during the extensive field work. Special thanks to Khoa Nguyen, Steven Beard, and Bruce Felt (and associates) for supporting the MARTE drill integration and to field team members of the robotics experiment: Scott Christa, Sara Huffman, Jen Jasper, Mark Branson, Thom Stone, Richard Alena, John Ossenfort, Steve Schultz, Kennda Lynch, Charlie Galindo, Michelle Goldschmid, Eric James, Erik Mumm, Tom Kennedy, Gale Paulsen, Jason Herman, Michael Rutberg, Josefina Torres Redondo, Eduardo Sebastian Martínez, Sara Navarro Lopez, and Mercedes Moreno Paz. The Museo Minero de Ríotinto provided critical field facilities and logistical support to the MARTE project. The Vazquez Díaz Hotel in Nerva, Spain provided additional logistical support, great meals, fabulous service, and a home away from home for the field team. Finally, the MARTE project would not have been possible without numerous contributions from Ricardo Amils and Todd Stevens. Gracias amigos.

Abbreviations

ASTEP, Astrobiology Science and Technology for Exploring Planets program; ATP, adenosine-5′-triphosphate; BHIS, Borehole Inspection System; BHIT, Borehole Inspection Tool; BHSP, Borehole Standard Probe; CCI, Core Context Imager; CORBA, Common Object Request Brokering Architecture; CRL, Contingent Rover Language; CSHS, Core Sample Handling System; DCSM, Drill Core Service Module; MARTE, Mars Astrobiology Research and Technology Experiment; MI, Microscopic Imager; MTP, Mars Technology Program; RLU, Relative Luminosity Unit; ROP, rate of penetration; RST, remote science team; VNIR, Visible–Near Infrared.

References

Amils, R., Gonzalez-Toril, E., Fernández-Remolar, D., Gomez, F., Aguilera, A., Rodriguez, N., Malki, M., Garcia-Moyano, A., Fairen, A.G., de la Fuente, V., and Sanz, J.L. (2007) Extreme environments as Mars terrestrial analogs: the Rio Tinto case. *Planet. Space Sci.* 55:370–381.

Arvidson, R.E., Anderson, R.C., Bartlett, P., Bell, J.F., III, Blaney, D., Christensen, P.R., Chu, P., Crumpler, L., Davis, K., Ehlmann, B.L., Fergason, R., Golembek, M.P., Gorevan, S., Grant, J.A., Greeley, R., Guinness, E.A., Haldemann, A.F.C., Herkenhoff, K., Johnson, J., Landis, G., Li, R., Lindemann, R., McSween, H., Ming, D.W., Myrick, T., Richter, L., Seelos F.P., IV, Squyres, S.W., Sullivan, R.J., Wang, A., and Wilson, J. (2004) Localization and physical properties experiments conducted by Spirit at Gusev crater. *Science* 305: 821–824.

Bonaccorsi, R. and Stoker, C.R. (2008) Science results from a Mars drilling simulation (Río Tinto, Spain) and ground truth for remote science observations. *Astrobiology* 8:967–985.

Boston, P.J., Ivanov, M.V., and McKay, C.P. (1992) On the possibility of chemosynthetic ecosystems in subsurface habitats on Mars. *Icarus* 95:300–308.

Boston, P.J., Spilde, M.N., Northup, D.E., Melim, L.A., Soroka, D.S., Kleina, L.G., Lavoie, K.H., Hose, L.D., Mallory, L.M., Dahm, C.N., Crossey, L.J., and Schelble, R.T. (2001) Cave biosignature suites: microbes, minerals and Mars. *Astrobiology* 1:25–55.

Boynton, W.V., Feldman, W.C., Squyres, S.W., Prettyman, T., Brückner, J., Evans, L.G., Reedy, R.C., Starr, R., Arnold, J.R., Drake, D.M., Englert, P.A.J., Metzger, A.E., Mitrofanov, I., Trombka, J.I., d'Uston, C., Wänke, H., Gasnault, O., Hamara, D.K., Janes, D.M, Marcialis, R.L., Maurice, S., Mikheeva, I., Taylor, G.J., Tokar, R., and Shinohara, C. (2002) Distribution of hydrogen in the near-surface of Mars: evidence for sub-surface ice deposits. *Science* 297:81–85.

Bresina, J., Golden, L.K., Smith, D.E., and Washington, R. (1999) Increased flexibility and robustness of Mars rovers. In *Proceedings of the 5th* International Symposium on Artificial Intelligence Robotics and Automation in Space, ESTEC, Noordwijk, The Netherlands, p 167.

Brown, A.J., Bishop, J.L., and Storrie-Lombardi, M.C. (2006) MR Prism—an image analysis tool and GIS for CRISM. *SPIE Optics and Photonics* 6309, doi:10.1117/12.677107.

Brown, A.J., Sutter, B., and Dunagan, S. (2008) The MARTE VNIR imaging spectrometer experiment: design and analysis. *Astrobiology* 8:1001–1011.

Bullock, M.A., Stoker, C.R., McKay, C.P., and Zent, A. (1994) A coupled soil-atmosphere model of H_2O_2 on Mars. *Icarus* 107:142–154.

Burt, D.M., Wohletz, K.H., and Knauth, L.P. (2006) Mars and mine dumps. *Eos, Transactions, American Geophysical Union* 87, doi:10.1029/2006EO490003.

Cannon, H., Stoker, C.R., Dunagan, S., Davis, K., Gomez-Elvira, J., Glass, B., Lemke, L.G., Miller, D., Bonaccorsi, R., Branson, M., Christa, S., Manfredi-Rodriguez, J.A., Mumm, E., Paulsen, G., Roman, M., Winterholler, A., and Zavaleta, J.R. (2007) MARTE: technology development and lessons learned from a Mars drilling mission simulation. *Journal of Field Robotics* 24:877–905.

Carr, M.H. (1996) *Water on Mars*, Boston University Press, New York.

Carvalho, D., Barriga, F.J.A.S., and Munhá, J. (1999) Bimodal-siliciclastic systems—the case of the Iberian pyrite belt. In *Volcanic-Associated Massive Sulfide Deposits: Processes and Examples in Modern and Ancient Settings*, edited by T. Barrie and M. Hannington, *Reviews in Economic Geology* 8:375–408.

Chapelle, F.H., O'Neill, K., Bradley, P.M., Methe, B.A., Ciufo, S.A., Knobel, L.L., and Lovley, D.R. (2002) A hydrogen-based subsurface microbial community dominated by methanogens. *Nature* 415:312–315.

Christensen, P.R. (2003) Formation of recent martian gullies through formation of extensive water-rich snow deposits. *Nature* 422:45–48.

Clifford, S.M. (2003) Mars H_2O: the limits of theoretical modeling and geomorphic interpretation in assessing the present distribution of subsurface H_2O on Mars [abstract 2118]. In *34th*Lunar and Planetary Science Conference, Lunar and Planetary Institute, Houston.

Clifford, S.M. and Parker, T.J. (2001) The evolution of the martian hydrosphere: implications for the fate of a primordial ocean and the current state of the northern plains. *Icarus* 154:40–79.

Des Marais, D.J., Allamandola, L.J., Benner, S.A., Boss, A.P., Deamer, D., Falkowski, P.G., Farmer, J.D., Hedges, S.B., Jakosky, B.M., Knoll, A.H., Liskowsky, D.R., Meadows, V.S., Meyer, M.A., Pilcher, C.B., Nealson, K.H., Spormann, A.M., Trent, J.D., Turner, W.W., Woolf, N.J., and Yorke, H.W. (2003) The NASA Astrobiology Roadmap. *Astrobiology* 3:219–235.

Fernández-Remolar, D.C., Rodríguez, N., Gómez, F., and Amils, R. (2003) The geological record of an acidic environment driven by iron hydrochemistry: the Tinto River system. *J. Geophys. Res*. 108, doi:10.1029/2002JE001918.

Fernández-Remolar, D.C., Gómez-Elvira, J., Gómez, F., Sebastian, E., Martin, J., Manffedi, J.A., Torres, J., Gonzales Kesler, C., and Amils, R. (2004) The Tinto River, an extreme environment under control of iron, as an analog of the Terra Meridiani hematite site of Mars. *Planet. Space Sci*. 52:239–248.

Fernández-Remolar, D.C., Morris, R.V., Gruener, J.E., Amils, R., and Knoll, A.H. (2005) The Rio Tinto Basin, Spain: mineralogy, sedimentary geobiology, and implications for interpretation of outcrop rocks at Meridiani Planum, Mars. *Earth Planet. Sci. Lett*. 240:149–167.

Fernández-Remolar, D.C., Prieto-Ballesteros, O., Rodríguez, N., Gómez, F., Amils, R., Gómez-Elvira, J., and Stoker, C.R. (2008) Underground habitats in the Río Tinto basin: a model for subsurface life habitats on Mars. *Astrobiology* 8:1023–1047.

Fisk, M.R. and Giovannoni, S.J. (1999) Sources of nutrients and energy for a deep biosphere on Mars. *J. Geophys. Res*. 104: 11805–11815.

Gómez, F., Fernández-Remolar, D.C., González-Toril, E.F., and Amils, R. (2004) The Tinto River, an extreme Gaian environment. In *Scientist on Gaia 2000*, edited by L. Margulis, J. Miller, P. Boston, S. Schneider, and E. Crist, MIT Press, Cambridge, MA, pp 321–334.

González-Toril, E.F., Llobet-Brossna, E., Casamayor, E.O., Amann, R., and Amils, R. (2003) Microbial ecology of an extreme acidic environment, the Tinto River. *Appl. Environ. Microbiol*. 69:4853–4865.

Haberle, R.M., McKay, C.P., Schaeffer, J., Cabrol, N.A., Grin, E.A., Zent, A.P., and Quinn, R. (2001) On the possibility of l iquid water on present-day Mars. *J. Geophys. Res*. 106: 23,317–23,326.

Hansen, C.J., Esposito, L., Stewart, A.I.F., Colwell, J., Hendrix, A., Pryor, W., Shemansky, D., and West, R. (2006) Enceladus' water vapor plume. *Science* 311:1422–1425.

Hansen, C.J., Bearman, G., Furstenau, S., Horn, J., Mahoney, C., Patrick, S., Peters, G., Scherbenski, J., Shiraishi, L., and Zimmerman, W. (2007) SPADE: a rock crushing and sample handling system developed for Mars missions. *J. Geophys. Res*. 112, doi:10.1029/2005JE002413.

Heldmann, J.L. and Mellon, M.T. (2004) Observations of martian gullies and constraints on potential formation mechanisms. *Icarus* 168:285–304.

Huffman, S., Glass, B.J. , Stoker, C., and Dashora, S. (2006) Remote science operations with a robotic Mars-prototype drilling platform [paper IAC-06-A5.P.05]. In *57th International Astronautical Congress,* International Astronautical Federation, Paris.

Jernsletten, J. (2005) Fast-Turnoff Transient Electromagnetic (TEM) field study at the Mars analog site of Río Tinto, Spain [abstract 1014]. In *36th Lunar and Planetary Science Conference,* Lunar and Planetary Institute, Houston.

Klein, H.P. (1979) The Viking mission and search for life on Mars. *Reviews of Geophysics and Space Physics* 17:1655–1662.

Klingelhöfer, G., Morris, R.V., Berhhardt, B., Schroder, C., Rodionov, D.S., de Souza P.A., Jr., Yen, A., Gellert, R., Evlanov, E.N., Zubkov, B., Foh, J., Bonnes, U., Kankeleit, E., Gutlich, P., Ming, D.W., Renz, F., Wdowiak, T., Squyres, S.W., and Arvidson, R.E. (2004), Jarosite and hematite at Meridiani Planum from Opportunity's Mössbauer spectrometer. *Science* 306: 1740–1745.

Laskar, J.A., Correia, C.M., Gastineau, M., Joutel, F., Levrard, B., and Robutel, P. (2004) Long term evolution and chaotic diffusion of the insolation quantities of Mars. *Icarus* 170:343–364.

LeGrand, R., Machulis, K., Miller, D.P., Sargent R., and Wright, A. (2005) The XBC: a modern low-cost mobile robot controller. In *Proceedings of Intelligent Robots and Systems, 2005*, IEEE/RSJ, doi:10.1109/IROS.2005.1545569.

Leistel, J.M., Marcoux, E., and Duchamps, Y. (1998) The volcano-hosted massive sulphide deposits of the Iberian pyrite belt. Review and preface to the thematic issue. *Mineralium Deposita* 33:82–97.

Lopez-Archilla, A.I., Marin, I., Gonzales, A., and Amils, R. (2001) Microbial community composition and ecology of an acidic aquatic environment. *Microbial Ecology* 41:20–35.

Maier, R.M. (2000) Biogeochemical cycling. In *Environmental Microbiology*, edited by R.M. Maier, I.L. Pepper, and C.P. Gerba, Academic Press, San Diego, pp 319–346.

Malin, M.C. and Edgett, K.S. (2000) Evidence for recent groundwater seepage and surface runoff on Mars. *Science* 288: 2330–2335.

Malin, M.C., Edgett, K.S., Posiolova, L.V., McColley, S.M., and Noe Dobrea, E.Z. (2006) Present-day impact cratering rate and contemporary gully activity on Mars. *Science* 314:1573–1577.

Mellon, M.T. and Phillips, R.J. (2001), Recent gullies on Mars and the source of liquid water. *J. Geophys. Res*. 106:1–15.

Miller, D.P., Bonaccorsi, R., and Davis, K. (2008) Design and practices for use of automated drilling and sample handling in MARTE while minimizing terrestrial and cross contamination. *Astrobiology* 8:947–965.

Murray, B.C., Ward, W.R., and Yueng, S.C. (1973) Periodic insolation variations on Mars. *Science* 180:638–640.

Nealson, K.H. (1997) The limits of life on Earth and searching for life on Mars. *J. Geophys. Res*. 102:23,675–23,686.

Pappalardo, R.T., Belton, M.J.S., Breneman, H.H., Carr, M.H., Chapman, C.R., Collins, G.C., Denk, T., Fagents, S., Geissler, P.E., Giese, B., Greeley, R., Greenberg, R., Head, J.W., Helfenstein, P., Hoppa, G., Kadel, S.D., Klaasen, K.P., Klemaszewski, J.E., Magee, K., McEwen, A.S., Moore, J.M., Moore, W.B., Neukum, G., Phillips, C.B., Prockter, L.M., Schubert, G., Senske, D.A., Sullivan, R.J., Tufts, B.R., Turtle, E.P., Wagner, R., and Williams, K.K. (1999) Does Europa have a subsurface

ocean? Evaluation of the geological evidence. *J. Geophys. Res*. 104:24,015–24,056.

Parro, V., Rodríguez-Manfredi, J.A., Briones, C., Compostizo, C., Herrero, P.L., Vez, E., Sebastián, E., Moreno-Paz, M., García-Villadangos, M., Fernández-Calvo, P., González-Toril, E., Pérez-Mercader, J., Fernández-Remolar, D.C., and Gómez-Elvira, J. (2005) Instrument development to search for biomarkers on Mars: terrestrial acidophile, iron-powered chemolithoautotrophic communities as model systems. *Planet. Space Sci*. 53:729–737.

Parro, V., Fernández-Calvo, P., Rodríguez Manfredi, J.A., Moreno-Paz, M., Rivas, L.A., García-Villadangos, M., Bonaccorsi, R., González-Pastor, J.E., Prieto-Ballesteros, O., Schuerger, A.C., Davidson, M., Gómez-Elvira, J., and Stoker, C.R. (2008) SOLID2: an antibody array-based life-detector instrument in a Mars drilling simulation experiment (MARTE). *Astrobiology* 8:987–999.

Pedersen, K. (2001) Diversity and activity of microorganisms in deep igneous rock aquifers of the Fennoscandian Shield. In *Subsurface Microbiology and Biogeochemistry*, edited by J.K. Fredrickson and M. Fletcher, Wiley-Liss, New York, pp 97–139.

Prieto-Ballesteros, O., Martínez-Frías, J., Schutt, J., Sutter, B., Heldmann, J.L., Bell, M.S., Battler, M., Cannon, H., Gómez-Elvira, J., and Stoker, C.R. (2008) The subsurface geology of Río Tinto: material examined during a simulated Mars drilling mission for the Mars Astrobiology Research and Technology Experiment (MARTE). *Astrobiology* 8:1013–1021.

Richardson, M.I. and Mischna, M.A. (2005) Long-term evolution of transient liquid water on Mars. *J. Geophys. Res*. 110, doi:10.1029/2004JE002367.

Sáez, R., Pascual, E., Toscano, M., and Almodovar, G.R. (1999) The Iberian type of volcano-sedimentary massive sulphide deposits. *Mineralium Deposita* 34:549–570.

Shock, E.L. (1997) High-temperature life without photosynthesis as a model for Mars. *J. Geophys. Res*. 102:23,687–23,694.

Sleep, N.H. and Zahnle, K. (1998) Refugia from asteroid impacts on early Mars and the early Earth. *J. Geophys. Res*. 103:28, 529–28,544.

Squyres, S.W. and Carr, M. (1986). Geomorphic evidence for the existence of ground ice on Mars. *Science* 231:249–252.

Stevens, T.O. (1997) Lithoautotrophy in the subsurface. *FEMS Microbiol. Rev*. 20:327–337.

Stevens, T.O. (2002) The deep subsurface biosphere. In *Biodiversity of Microbial Life*, edited by J.T. Staley and A.L. Reysenbach, Wiley-Liss, New York, pp 439–474.

Stevens, T.O. and McKinley, J.P. (1995) Lithoautotrophic microbial ecosystems in deep basalt aquifers. *Science* 270:450–454.

Stevens, T.O. and McKinley, J.P. (2000) Abiotic controls on H_2 production from basalt-water reactions and implications for aquifer biogeochemistry. *Environ. Sci. Technol*. 34:826–831.

Stoker, C.R., Dunagan, S., Stevens, T., Amils, R., Gómez-Elvira, J., Fernández, D., Hall, J., Lynch, K., Cannon, H., Zavaleta, J., Glass, B., and Lemke, L. (2004) Mars Analog Río Tinto Experiment (MARTE): 2003 drilling campaign to search for a subsurface biosphere at Río Tinto, Spain [abstract 2025]. In *35th Lunar and Planetary Science Conference,* Lunar and Planetary Institute, Houston.

Stoker, C.R., Stevens, T., Amils, R., Gomez-Elvira, J., Rodriguez, N., Gomez, F., Gonzales-Toril, E., Aguilera, A., Fernández-Remolar, D., Dunagan, S., Lemke, L.G., Zavaleta, J., and Sanz, J.L. (2005), Characteriztion of a subsurface biosphere in a massive sulfide deposit at Rio Tinto, Spain: implications for extant life on Mars [abstract 1534]. In *36th Lunar and Planetary Science Conference,* Lunar and Planetary Institute, Houston.

Sutter, B., Brown, A., and Stoker, C.R. (2008) Visibile–near infrared point spectroscopy of drill core samples from Río Tinto, Spain: results from the 2005 Mars Astrobiology Research and Technology Experiment (MARTE) drilling exercise. *Astrobiology* 8:1049–1060.

Takai, K., Moser, D.P., DeFlaun, M., Onstott, T.C., and Fredrickson, J.K. (2001) Archaeal diversity in waters from deep South African gold mines. *Appl. Environ. Microbiol*. 67:5750–5760.

Winterholler, A., Roman, M., Miller, D.P., Krause, J., and Hunt, T. (2005) Automated core sample handling for future Mars drill missions. In *Proceedings of the 8th International Symposium on Artificial Intelligence, Robotics and Automation in Space,* edited by B. Battrick, ESA Publications, ESTEC, Noordwijk, the Netherlands.

Zacny, K.A., Quayle, M.C., and Cooper, G.A. (2004) Laboratory drilling under martian conditions yields unexpected results. *J. Geophys. Res*. 109, doi:10.1029/2003JE002203.

Zent, A.P. and McKay, C.P. (1994) The chemical reactivity of the martian soil and implications for future missions. *Icarus* 108:146–157.

Address reprint requests to:
Carol Stoker
Mail Stop 245-3
NASA Ames Research Center
Moffett Field, CA 94035

E-mail: cstoker@mail.arc.nasa.gov